OBJECT–ORIENTED HYDROLOGIC MODELING WITH GIS

A Dissertation

Submitted to the Faculty

of

Purdue University

by

Kwangmin Kang

In Partial Fulfillment of the

Requirements for the Degree

of

Doctoral of Philosophy

May 2011

Purdue University

West Lafayette, Indiana

To my wife, my daughter, my son, my parents and the rest of my family.

ACKNOWLEDGMENTS

I would like to thank all of those who have encouraged, helped, and supported me during my doctorate. First of all, I would like to thank my Ph.D. advisor, Professor Venkatesh Merwade, for his support and encouragement over the past four years. I also express my gratitude to my Ph.D. committee members, Professor Rao Govindaraju, Professor Bernard Engel and Professor Dennis Lyn, for their guidance and encouragement during Ph.D. research. Especially, I also appreciate Dr. Shivam Tripathi for his continuous help. Finally, thanks are due to hydrology secretary, Mrs. Judith Haan, and all my colleagues.

TABLE OF CONTENTS

Page

Page

LIST OF TABLES

Table Page

LIST OF FIGURES

Figure Page

ABBREVIATIONS

HEC–HMS	Hydrologic Engineering Center Hydrologic Modeling System
GIS	Geographic Information System
DEM	Digital Elevation Model
GHISMO	GIS and Hydrologic Information System Modeling Objects
STORE DHM	Store Released Based Distributed Hydrologic Model
SHE	Système Hydrologique Europèen
IHDM	Institute of Hydrology Distributed Model
CSIRO TOPOG	Terrain Analysis Hydrologic Model
SDDH	Spatially Distributed Direct Hydrograph Travel time method
RAS	River Analysis System
SWAT	Soil Water Assessment Tool
WMS	Watershed Modeling System
Z–R	Reflectivity – Rainfall
HDP	Hourly Digital Precipitation
NEXRAD	Next Generation Radar
CONUS	Covering the entire Continental United States
RFC	River Forecast Center
MPE	Multisensor Precipitation Estimator
NWS	National Weather Service
GOES	Geostationary Operational Environmental Satellite
SCS	Soil Conservation Service
CN	Curve Number

CCT	Critical Cell Travel Time
AR1	Autoregressive Order One
MFB	Mean Field Bias
IDW	Inverse Distance Weight
HRAP	Hydrologic Rainfall Analysis Project
NLCD	National Land Cover Dataset
USGS	United States Geological Survey
NRCS	National Resources Conservation Service
OHRFC	Ohio River Forecast Center
UWR	Upper Wabash River Basin
UCR	Upper Cumberland River Basin
E_{NS}	Nash Sutcliffe efficiency coefficient
R^2	Co–efficient of determination
RMSE	Root Mean Square Error
MAPE	Mean Absolute Percentage Error
SNU–R	Spatially non–uniform NEXRAD bias correction with rain gauge interpolation
SNU–E	Spatially non–uniform NEXRAD bias correction with radar bias interpolation

ABSTRACT

Kang, Kwangmin. Ph.D., Purdue University, May 2011. Object–oriented Hydrologic Modeling with GIS. Major Professor: Venkatesh Merwade.

A prototype geographic information system (GIS) based tightly coupled object oriented framework called GIS and Hydrologic Information System Modeling Object (GHISMO) is presented in this thesis. The proposed GHISMO framework is developed within ArcGIS environment such that geographic datasets can be treated as hydrologic objects that have properties and methods to simulate a hydrologic system. The overall GHISMO framework consists of HydroShed as a super class which is composed of six sub classes, namely, HydroGrid (for grid based data such as digital elevation model), ParameterGrid (for grid based parameters such as land use type), HydroArea (for polygon features such as lakes and reservoirs), HydroCatchment (for polygon features representing catchments and watersheds), HydroLine (for polyline features such as rivers) and HydroTable (for input and output tabular data). The GHISMO framework is applied to develop a modular hydrologic modeling system called the Storage Release based Distributed Hydrologic Model (STORE DHM). The storage–release concept uses the travel time within each grid cell to compute how much water is stored or discharged to the watershed outlet at each time step. The STORE DHM is tested by simulating multiple hydrologic events in three watersheds in Indiana. In addition, the GHISMO framework is tested for its flexibility to adopt additional modules by implementing three rainfall bias correction methods to provide accurate input for the STORE DHM.

Application of STORE DHM to multiple hydrologic events in three different watersheds in Indiana show that the model is able to predict runoff hydrographs for different types of events in terms of storm duration, peak flow magnitude and time–to–peak. In addition, STORE DHM output is compared with outputs from two hydrologic

models including Hydrologic Engineering Center's Hydrologic Modeling System (HEC–HMS) and time variant Spatially Distributed Direct Hydrograph travel time method (SDDH). Results from these comparisons show that the STORE DHM outperforms both HEC–HMS and SDDH in terms of overall hydrograph shape and flow magnitude.

The flexibility of GHISMO framework is tested by extending it to include a rainfall bias correction module. The rainfall bias correction module is then used to correct NEXRAD radar rainfall by implanting two non–uniform bias correction techniques. Results from STORE DHM simulations using the original NEXRAD rainfall and bias-corrected rainfall created in this study shows that the model response is dictated by rainfall variations in the study area. The performance of STORE DHM output is relatively better in a larger watershed with high variable rainfall compared to a smaller watershed with uniform rainfall pattern. The findings from this study are limited by the number of watersheds used, and the quality of the data. More testing of the GHISMO framework and its modules is needed to make the proposed framework applicable for different watersheds with varying scales.

CHAPTER 1. INTRODUCTION

1.1. Background

The hydrologic system is dynamic; states of the system are frequently updated as meteorological inputs and basin characteristics change. Modeling this dynamic behavior imposes special requirements on data handling and process calculations that make development of event–based hydrologic model a challenging task. In the past two decades, many event–based hydrologic models have been developed such as HEC–HMS (Hydrologic Engineering Center–Hydrologic Modeling System), VIC (Variable Infiltration Capacity), DRAINMOD and Vflo^{TM} (Vieux, Inc.). Nevertheless, most of the existing models have limitations in representing hydrologic processes and therefore they cannot guarantee realistic simulations. For example, HEC–HMS is a lumped model – it does not account for spatial variations in hydrologic processes. Further, most of the existing models are not standalone (they need external software to get data or to run simulation, e.g. Vflo^{TM}) which makes them unwieldy. In addition, these existing models are also inflexible for investigating hydrological processes because it is difficult to add new hydrological components in them. To overcome these limitations, this study develops GIS and Hydrologic Information System Modeling Object (GHISMO), an event–based distributed hydrologic model, in a single platform of ArcGIS software. The GHISMO uses object–oriented programming approach which provides flexibility in investigating new hydrologic processes without changing the basic model framework. The objectives of this research are – (1) to make a prototype of an object–oriented hydrologic model framework (called GHISMO); (2) to investigate the robustness of the

developed prototype framework through several case studies; and (3) to demonstrate the flexibility of the modeling framework in overcoming critical modeling hurdles.

1.2. Literature Review and Motivation

1.2.1. Hydrologic Model

Watershed based hydrologic models are important tools in operational hydrology and water resources planning and management. A watershed scale hydrologic model is a simplified description of the hydrologic system of a watershed. Traditionally, statistical and conceptual hydrologic models have treated input parameters as lumped over the entire study watershed by ignoring the spatial variability of the physical system and its processes. Specifically, these models cannot accurately represent and model the spatial variation in meteorological and land surface conditions that affect various hydrologic processes, and therefore cannot assure realistic simulations. With the availability of DEM (Digital Elevation Model) and next generation radar (NEXRAD) rainfall data, grid based hydrologic models are more effective in representing the variations of meteorological forcing and land surface parameters. Also, geographic information system (GIS) allows processing of grid and vector data, which has led to rapid progress in distributed hydrologic modeling. However, an existing problem in hydrologic modeling is that the available software for handling spatial information and for running model simulation is not integrated in the same environment.

An object–oriented approach to hydrologic modeling increases model flexibility and reduces efforts when adapting the model for new application, area and algorithm. Rather than replacing an old code that already works, the model code can be extended using the object–oriented *characteristic of inheritance* (Kiker et al., 2006). An object–oriented approach allows for building an incremental model that can be adapted to

different watershed conditions (Wang et al., 2005). In spite of many advantages, the object–oriented approach has found only limited applications in hydrologic modeling (Band et al., 2000; Kralisch et al., 2005; Lal et al., 2005). Band et al. (2000) describes a spatial object–oriented framework for modeling watershed systems to include hydrological and ecosystem fluxes. Chen and Beschta (1999) developed a 3–dimensional distributed hydrological model–OWLS (the Object Watershed Link Simulation model) for dynamic hydrologic simulation and applied it to the Bear Brook watershed in Maine. Garrote and Becchi (1997) employs object oriented programming techniques with distributed hydrologic models for real–time flood forecasting. Boyer et al. (1996) presents an object–oriented method to simulate a rainfall–discharge relationship using a lumped hydrologic model. McKim et al. (1993) introduced an object–oriented approach to simulate hydrologic processes, specifically infiltration excess overland flow. The above applications used object–oriented approach and achieved reasonable results for hydrologic simulations. However, object–oriented approach is not comprehensively discussed in the hydrologic literature and no general guideline exists for implementing them in hydrologic models (Wang et al., 2005 and Kiker et al., 2006).

With the advent of remote sensing technology in topography analysis, several distributed grid–based hydrologic models have been developed. These include SHE (Système Hydrologique Europèen, Abbott et al., 1986), IHDM model (Institute of Hydrology Distributed Model, Calver and Wood, 1995), the CSIRO TOPOG model (Terrain Analysis Hydrologic Model, Vertessy et al., 1993) and HILLFLOW (Bronstert and Plate, 1997). These models use grid–based routing (kinematic wave or diffusive wave) approach to account for spatio–temporal variations in water movement. However, they use complex algorithms with low computational efficiency requiring a large data base for calibration and large computational resources for simulation (Beven, 2001). Recently, several event–based grid models have been developed that use travel time method for routing the flow through a watershed. These include: (i) the spatially distributed unit hydrograph method by Maidment et al., (1993, 1996; Muzik 1995; Ajward, 1996), (ii) the first passage–time response function which is derived from the advection–dispersion method by Olivera and Maidment (1999), (iii) diffusive transport

method by Liu et al. (2003), and (iv) spatially distributed travel time method by Melesse and Graham (2004), among others. Maidment (1993) assumed a time–invariant velocity to get the unit hydrograph; whereas Muzik (1995) and Ajward (1996) used continuity and Manning's equations to determine the flow velocity through each cell. Melesse and Graham (2004) propose an integrated technique using remote sensing and GIS datasets to compute spatially distributed excess rainfall, which was then routed by using the travel time concept without relying on the unit hydrograph theory. Although these techniques provided satisfactory results, the flow from each grid cell is routed through the system independently without considering the interaction of neighboring cells as the water flows downstream.

1.2.2. The problem of rainfall uncertainty for hydrologic model

Rainfall is a critical factor in hydrologic simulation. However, rainfall varies substantially in space and time and therefore it is often poorly represented in hydrologic models. Numerous studies in the past decades have investigated the sensitivity of runoff hydrographs to spatial and temporal variations in precipitation. Faures et al. (1995) concluded that for realistic hydrologic simulations, even for small watersheds, hydrologic models require detailed information of the spatial rainfall patterns. This result agreed with Wilson et al. (1979), who showed that the spatial distribution of rainfall had a marked influence on the runoff hydrograph from a small catchment. Troutman et al. (1989) investigated the effect of rainfall variability on model simulation, and concluded that improper representation of rainfall variability over a basin would lead to overestimation or underestimation of runoff.

Combining radar and gauge information produces improved precipitation estimates, in terms of both quality and spatial resolution, in comparison with either radar or gauge estimates alone (Smith and Krajewski, 1991). However, uncertainty persists in MPE (Multisensor Precipitation Estimator) products because large portions of the radar

coverage area do not have rain gauge data to adjust biases in radar rainfall (Ciach and Krajewski, 1999). Habib et al. (2009) studied a small watershed with dense rain gauge network in south Louisiana and found that the MPE products tend to overestimate small rain rates and underestimate large rain rates. They suggested that dense rain gauge observations can improve MPE performance; however, maintaining a dense rain gauge network in a large catchment is costly and impractical.

Winchell et al. (1998) investigated the effects of uncertainty in NEXRAD estimated precipitation input on simulation of runoff. Specifically, they studied the sensitivity of surface runoff to uncertainty in precipitation estimates arising from the transformation of radar reflectivity to precipitation rate and from spatio–temporal aggregation of the precipitation field. They found that the *infiltration–excess mode* of surface runoff generation is more sensitive to precipitation uncertainties than the *saturation–excess mode* of surface runoff generation. The study concluded that a limited number of rain gauges may not completely eradicate biases in the radar data and may lead to poor runoff simulations. In recent years, the availability of high–resolution precipitation data from different weather radar platforms has intensified the research on understanding the effects of spatial resolution in precipitation data on hydrologic simulations.

1.2.3. The problem of DEM variations for hydrologic model

Topographically–based modeling of catchment processes is becoming popular in applied environmental research, mainly due to the advances in availability and quality of DEM (Moore et al., 1991; Goodchild et al., 1993; Wise, 2000). Presently, DEM is used in terrain modeling applications such as distributed hydrologic models (Beven and Moore, 1993), prediction of surface saturation zones (O'Loughlin, 1986), erosion deposition models (Desmet and Govers, 1996; Schoorl et al., 2000), and hillslope stability and landslide hazard models (Montgomery and Dietrich, 1994; Tarboton, 1997). Analysis in

DEM include automatic delineation of catchment areas (O'Callaghan and Mark, 1984; Martz and De Jong, 1998), development of drainage networks (Fairfield and Leymarie, 1991), detection of channel heads (Montgomery and Dietrich, 1994), determination of flow accumulation (Peuker and Douglas, 1975), and flow direction and routing (Tarboton, 1997). Wilson et al. (2000) demonstrated that (a) slope gradient and specific area of the catchment tend to decrease as DEM cell size increases, (b) larger DEM cell sizes produce shorter total flow length in a watershed, and (c) the accuracy of slope gradient decreases with increase in DEM cell size. The DEM resolution is expected to affect the delineation of watersheds which in turn would influence hydrologic model performance (Madsen, 2003). However, the effect of DEM resolution on the performance of a hydrologic model is not yet well understood (Vazquez et al., 2004).

Zhang and Montgomery (1994) used DEM of different resolutions in conjunction with *eight flow–direction* algorithms to detect patterns in storm runoff and surface saturation. They found that DEM sizes significantly affect computed topographic parameters and hydrographs in TOPMODEL simulation. Studying a watershed in Iowa using KINEROS (kinematic runoff and erosion model) Kalin et al. (2003) observed that increasing the DEM resolution increases the magnitude of peak flow without affecting its time of occurrence. FitzHugh and Mackay (2000) investigated a watershed in Wisconsin using SWAT (Soil and Water Assessment Tool) and observed that sediment yield from a watershed delineated using a fine resolution DEM (10m) dropped by 44% in comparison to a watershed delineated using a coarse resolution DEM (500m). All the aforementioned studies on DEM found that the DEM resolution significantly affects the computation of slope, catchment area, flow direction and surface runoff. Thus hydrologic model simulations are very sensitive to DEM resolution.

1.3. Objective of the study

The overall goal of this research effort is to develop an efficient and robust event–based distributed hydrologic model under ArcGIS environment that can overcome some of the existing hurdles of hydrologic modeling through an object–oriented approach. To accomplish this objective, the following tasks were executed:

(1) Develop a prototype of GIS based object–oriented framework for hydrologic modeling.

(2) Test robustness of the developed prototype by applying it to various storm events over different study areas.

(3) Demonstrate the flexibility of developed prototype in linking additional objects/modules to it.

The remainder of this dissertation is structured as follows. In Chapter 2, description of the GHISMO diagram is introduced. In Chapter 3, development and application of grid–based distributed hydrologic model is presented. Chapter 4 presents the implementation module for correcting spatially distributed rainfall bias.

CHAPTER 2. GIS AND HYDROLOGIC INFORMATION SYSTEM MODELING OBJECT

2.1. Introduction

Computer based models have been used as planning tools in water resources management over the last three decades. The researches in computational water resources are well known and organized. Also, many models are applied to resolve a variety of hydrologic components (Abbott et al., 1993). It is necessary to combine several of these models (e.g., surface water model, groundwater model and reservoir model) to bring a holistic idea in water resources planning and management. Realization of this approach requires a modular structure in water resources research, and it allows different sub–models to be interconnected depending on the hydrologic system. Another important aspect that must be considered in new development of hydrologic models is creating software elements that can be adapted in future projects. If a modular structure provides reusable components, both regarding development time and reliability of the software produced, it will be an extensive water resources platform (Goldberg et al., 1995). This also will reduce development and maintenance cost for the project.

Running a hydrologic model involves several steps including data collection, pre–processing, parameter estimation, calibration and validation. With the advancement in data collection methods and their representation in digital form, the use of GIS is common for data management, pre–processing and post–analysis in any hydrologic modeling study (Maidment, 1993). While GIS provides a user friendly visual environment for handling hydrologic data, it lacks the computational engine to perform hydrologic simulations. Also, many hydrologic models have limitations of GIS

capabilities for data handling, pre–processing and visualization. As a result, several efforts have been made to couple GIS with hydrologic models. These efforts include: (i) the development of GIS tools for Hydrologic Engineering Center's (HEC) Hydrologic modeling system (HMS) and River Analysis System (RAS) models [U.S. Army Corps of Engineers (USACE)]; (ii) the integration of GIS and modeling tools in EPA BASINS analysis environment (Lahlou et al., 1998); (iv) the development of a GIS pre–processor for the Soil Water Assessment Tool (SWAT; Luzio et al., 2002); and (v) the development of Watershed Modeling System (WMS; Environmental Modeling Research Laboratory, Nelson 1997).

Most previous attempts listed above to link GIS and hydrologic models can be categorized as 'loosely coupled' because both systems act independent of each other, and are only linked through input or output data. For example, GIS tools are used to develop the input file, which is then used to run the hydrologic model. Any changes in the model domain or input attributes during the modeling process are not reflected in the data that are used in creating the model input. With the availability of high resolution geospatial and temporal data, and improved capability of GIS to handle continuous, dynamic datasets including time series, it is now possible to expand the role of GIS beyond that of a pre– or post–processing tool for hydrology to a tightly coupled modeling environment where GIS can perform hydrologic simulations.

If a hydrologic model investigates a new hydrologic component within the frame, an object–oriented approach allows for increased model flexibility without changing the main frame. The model codes that already exist in the old module can be extended by using the inheritance characteristic through an object–oriented approach (Kiker et al., 2006). In recent years, object–oriented based hydrologic models are increasingly used in water resources research, and also the modeling paradigm in water resources is changing to the object–oriented approach (Wang et al., 2005). Creating an incremental watershed model can be made by object–oriented design methods and using an object–oriented programming language (Wang et al., 2005), and this model can be applied to various watershed conditions. Even though object–oriented based hydrologic models have attractive advantages, few object–oriented based hydrologic models exist, and there is no

detailed discussion for the principle of object–oriented hydrologic approach (e.g. Band et al., 2000; Kralisch et al., 2005; Lal et al., 2005).

The most advanced water resources modeling research is increasing model flexibility to consider comprehensive natural phenomena. In addition, constructing this model can promote an extension of new hydrologic components by reducing inefficient efforts. This research presents the development of a new prototype hydrologic model frame, GIS and Hydrologic Information System Modeling Object (GHISMO), developed with an object–oriented approach. It should be noted that the objective of this work is not to create another model, but to create a framework where different models or their components can interact with each other within a GIS environment to overcome hydrologic modeling issues through an object–oriented approach.

2.2. Object Orientation in Hydrology

According to Bian (2007), object orientation involves three levels of abstractions: object oriented analysis, object oriented design, and object oriented programming. Object oriented analysis involves conceptual representation of the world including the facts and relationships about a situation. In hydrology, this would mean the conceptual representation of a watershed as a set of objects to include streams and corresponding catchments. Object oriented design uses the conceptual representation from object oriented analysis to create a formal model of objects, their properties, events, and relationships. Object oriented programming involves the implementation of objects and their events to accomplish a certain task. Object orientation relies on two basic principles: encapsulation and composition. Encapsulation considers that the world is composed of objects, and that each object has an identity, properties and behavior. The properties of an object are defined by its attributes (e.g., length, area), and the behavior is represented by methods. While the value of an attribute can define the state of an object, a method can change the state of an object, and that change is referred to as an event. For example, a

river object will have properties such as length and slope, methods such as RouteFlow and ComputeStorage, and routing a hydrograph through the river (by using RouteFlow method) is an event.

The principle of composition describes how objects are related through relationships including inheritance, aggregation and association. In object orientation, all objects belong to object classes, and all classes are hierarchal. A sub-class is a kind of this own super-class (through inheritance) and inherits all properties and methods from the super class, but also may have its own additional properties and methods. An object can also be a part of another object (through aggregation), and can simultaneously maintain relationships with other objects (through association). For example, an AlluvialRiver class can be a sub–class of River super class (inheritance), a River class can be a part of RiverNetwork class (aggregation) and River class is related with Watershed class through streamflow (relationship). Past studies that used object orientation for hydrologic modeling include Whittaker et al. (1991) who used object–oriented approach to model infiltration excess overland flow. Boyer et al. (1996) used object oriented approach to develop a lumped rainfall–runoff model. McKim et al. (1993) used object orientation to combine remote sensing and hydrologic data to develop a forecast model. Garrote and Becchi (1997), Band et al. (2000), and Wang et al (2005) proposed object oriented frameworks for modeling hydrologic processes at watershed scale. Most of these studies used object orientation to model hydrologic processes using the concepts of inheritance and aggregation. Recently, Richardson et al. (2007) proposed a prototype geographically based object framework for linking hydrologic and biochemical processes in the sub–surface. The process objects, however, were loosely coupled with geographic objects, thus leaving an opportunity for a tightly coupled geographically based object oriented modeling.

Relatively recent advances in GIS have enabled adaption of object orientation in storing and handling geospatial and temporal hydrologic data in research and practice. For example, Arc Hydro (Maidment, 2002) uses an object oriented approach to represent hydrologic environment through feature, object and relationship classes within a geodatabase. In Arc Hydro, a HydroEdge (stream) is sub class of generic Polyline super

class (inheritance), and is a part of HydroNetwork (aggregation). HydroEdge is related to Watershed (which itself is a sub–class of Polygon super class) through a common identifier (HydroID). Thus, ArcHydro uses object orientation to develop a physical representation of hydrography by using GIS objects. Thus, by knowing the HydroID of any geographic feature, it is possible to trace the flow of water by using points, lines, and polygons at multiple scales including at continental scale. The National Hydrography Dataset (NHD) available for the entire United States from the United States Geological Survey (USGS) also uses the object oriented (or geodatabase) design to provide data to its users.

The geodatabase approach to hydrology data overcomes several practical issues which are associated with storing and handling heterogeneous multi–scale data by providing a relational data model. Besides overcoming the data issues, the geodatabase approach provides an opportunity to exploit the potential of object oriented approach to overcome the limitations of scale and parameterization in distributed modeling of hydrologic processes. For example, if a polygon representing a watershed in GIS is treated as a hydrologic object that has some properties (e.g. area and slope) and methods (to compute runoff and route flow), then multiple watersheds can be linked and executed in parallel to scale–up the modeling domain from one single watershed to larger (national or continental) scales. Similarly, the availability of increasing GIS layers to represent soil, landuse and topography at multiple scales, can enable parameterization of hydrologic processes (or watershed methods) through GIS tools, which is not possible with most existing models that do not explicitly work within a GIS environment. This research builds on past studies to create a prototype tightly coupled object oriented GIS based hydrologic model to simulate hydrologic processes using geospatial inputs. The prototype modeling approach presented in this research is developed by using Visual Basic and ArcObjects within ArcGIS, and is referred to as GIS and Hydrologic Information System Modeling Objects (GHISMO).

2.3. Hydrologic Modeling Objects

An object–oriented hydrologic model framework is implemented in ArcGIS by developing hydrologic modeling objects as shown in Fig. 2.1. The hydrologic modeling object framework implements both principles of aggregation (represented with diamond) and inheritance (represented with triangle arrow) as shown in Fig. 2.1. HydroShed is the highest level class that includes the following six classes: (1) HydroGrid (to process gridded hydrologic information such as topography and rainfall), (2) ParameterGrid (to process gridded hydrologic parameters such as Mannings n), (3) HydroArea (to process vector hydrologic data for lakes and rivers), (4) HydroCatchment (to process vector hydrologic data for catchments or sub–watersheds), (5) HydroLine (to process vector hydrologic data for streams), and (6) HydroTable (to process tabular data). As displayed in Fig. 2.1, those classes dealing with raster, vector and tables are implemented in this research.

ProcessGrid (to implement hydrologic processes) and TopoGrid (to implement terrain processes) are two sub–classes of the HydroGrid class. ProcessGrid can work on gridded data to implement hydrologic processes to create excess rainfall and runoff hydrograph by implementing specific sub–classes such as ExRain and Hydrograph as shown in Fig. 2.1. ExRain implements specific techniques such as SCS curve number (through SCS sub–class) and Green–Ampt (through GreenAmpt sub–class) to compute excess rainfall using the rainfall input. Hydrograph class implements specific techniques such as storage release to compute runoff hydrograph from excess rainfall. TopoGrid implements sub–classes to create terrain attributes such as flow direction, flow accumulation, stream network and catchment by using topography data (DEM).

HydroArea can work on flow transformation by implementing specific techniques such as SCS dimensionless unit hydrograph (through SCSUnit sub–class) and Clark unit hydrograph (through ClarkUnit sub–class) for vector data. Also, HydroLine can work on river routing by implementing specific techniques such as Kinematic wave river routing (through KinematicWave sub–class) and Muskingum river routing (through Muskingum sub–class).

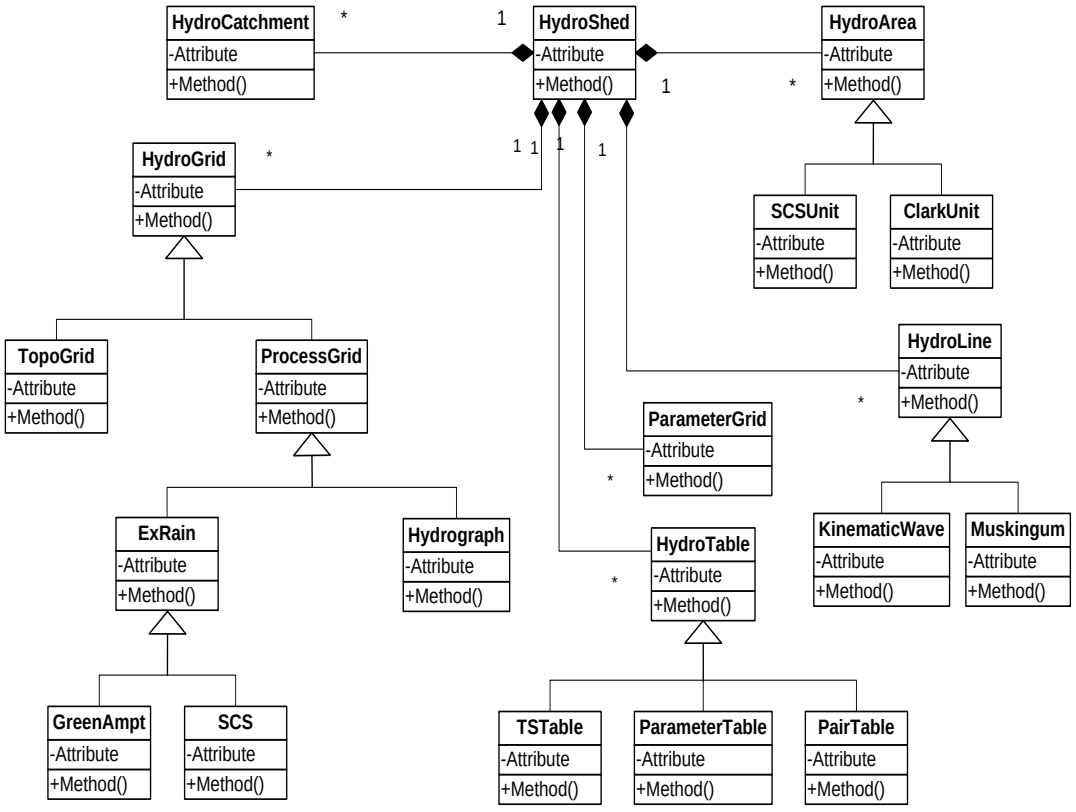

Figure 2.1 Object Model Diagram for GHISMO.

HydroTable implements three tables: TSTable, ParameterTable and PairTable. TSTable class processes time series table (e.g., rainfall and streamflow time series); ParameterTable processes parameter values linked to geographic features (e.g., Manning's n values for different land cover types); and PairTable processes paired data such as stage–discharge rating curves.

2.4. Updating the GHISMO Framework

An object in GHISMO allows creating a class or a function to handle a variety of hydrologic components. The GHISMO provides flexibility in modular development of the model without changing the basic framework through object–oriented approach, if hydrologic mechanisms need more advanced investigations. For example, this research creates a new object, RadarBias (to implement three different radar bias correction processes), to investigate the effect of different radar bias corrected rainfall inputs on hydrologic simulations as shown in Fig. 2.2. The GHISMO allows adding a RadarBias object that is a part of the new modeling processes without changing its main framework because the GHISMO is designed to be open to extension. The greatest benefit in the application of this design approach (open for extension for modification) is reusability and maintainability, and its advantages can overcome a prospective hydrologic modeling issue, such as making a large and complex hydrologic model. Specific methodology and application of hydrologic modeling as a part of the GHISMO framework are described in Chapter 3, and methodology and application of updating RadarBias object are also described in Chapter 4.

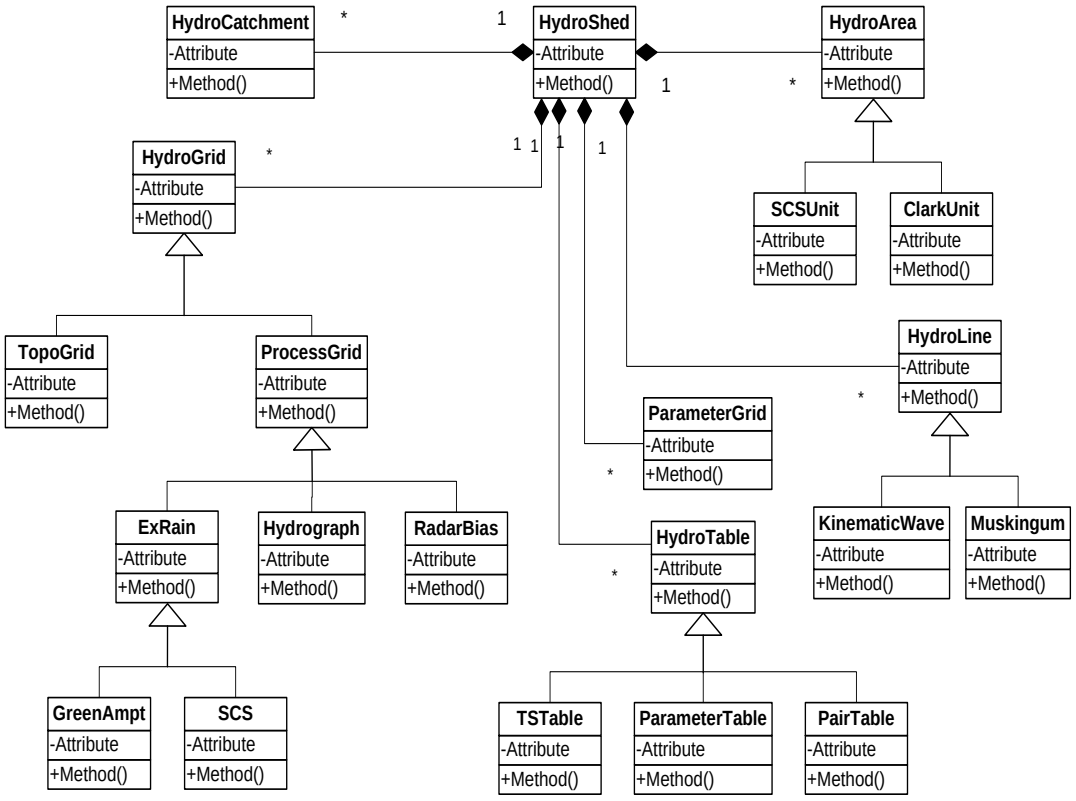

Figure 2.2 Update Object Model Diagram for GHISMO.

CHAPTER 3. DEVELOPMENT AND APPLICATION OF A STORAGE–RELEASE BASED DISTRIBUTED HYDROLOGIC MODEL USING GIS

3.1. Introduction

Hydrologic model development is complicated by the nonlinear, time dependent and spatially varying nature of rainfall–runoff mechanism (Remesan, 2009). The rainfall–runoff process is affected by many factors such as rainfall dynamics, topography, soil type and land use. Significant advancements in hydrological modeling started with the introduction of unit hydrograph model and its related impulse response function (Sherman, 1932). Since then, a myriad of hydrologic models have been developed, calibrated and validated for several watersheds at different scales. Developing a realistic hydrologic model requires an understanding of the interrelation between parameterization and scale because as the scale of the hydrologic modeling problem increases, the complexity of the model increases as well (Famiglietti, 1994).

The commonly used HEC–HMS (Hydrologic Engineering Center Hydrologic Modeling System; USACE, 1998) model does not account for spatial variations in hydrologic processes because it is a lumped hydrologic model which treats input parameters as an average over the watershed. In addition, use of HEC–HMS requires external software such as HEC–GeoHMS to produce necessary input files for the model. HEC–GeoHMS is an ArcGIS toolbar to process digital information related to topography, land use, and soil to produce input files for HEC–HMS. Because of their simplicity in terms of data requirements, model parameterizations and application, lumped hydrologic models such as HEC–HMS have been very popular in hydrology.

Application of semi–distributed or distributed models is complicated due to data requirements for physically based models (Koren et al., 2003), and parameter estimation for conceptual models (Moreda et al., 2006). To fully exploit the strength of semi–distributed and distributed models, it is necessary to provide data that can capture the spatio–temporal variations in the hydrologic system including rainfall dynamics. Difficulties related to data requirements for spatially distributed hydrologic models are addressed by the availability of continuous digital data in the form of digital elevation model (DEM) and gridded radar rainfall. In addition to the availability of geospatial data, the use of geographic information system (GIS) to process grid and vector data has led to rapid progress in grid based distributed hydrologic modeling (e.g., Maidment, 1993; Olivera and Maidment, 1999; Melesse et al., 2004). The use of spatially distributed topographic, soils, land use, land cover, and precipitation data in GIS ready format provides the framework for the development, verification, and eventual acceptance of new hydrologic models capable of taking full advantage of these new data, while acknowledging the uncertainty inherent in the data.

The broader goal of this study is to create a conceptual hydrologic model framework, called GIS and Hydrologic Information System Modeling Objects (GHISMO), which can utilize GIS data at different resolutions, and use these data to simulate hydrologic processes at multiple scales. GHISMO is expected to provide a platform where different models or their components can interact with each other within a GIS environment to overcome the issues related to computational requirements, scale and versatility through an object oriented design. As a first step towards accomplishing this broader goal, this chapter presents the development and application of a prototype grid based hydrologic model using object oriented programming concepts. The data and computational side of GHISMO is developed by using ArcObjects (building blocks or objects of the ArcGIS software), and the conceptual model for hydrologic simulations is based on a simple storage–release approach. In the storage–release approach, each cell in a raster grid provides storage for the water draining to it from neighboring cells, and then the water is released to downstream cells based on the travel time computed by combining the continuity and Manning's equations. This chapter specifically presents the

conceptual framework of the prototype hydrologic model, and its application to three study sites in Indiana. The grid based hydrologic model will be referred as the Storage Released based Distributed Hydrologic Model (STORE DHM).

3.2. Background and Related Work

Maidment (1993) proposed a time–area method within raster GIS to derive a spatially distributed unit hydrograph. Maidment's method uses a DEM to determine the flow direction from each cell based on the maximum downhill slope, and flow velocity through each cell is estimated based on the kinematic wave assumption. The travel time through each cell is then obtained by dividing the flow distance by the flow velocity. Maidment demonstrated that if a constant velocity can be estimated for each grid cell, a flow time grid can be obtained and subsequently isochronal curves and a time–area diagram can be determined for a watershed. Maidment's method is based on velocity time invariance in a linear hydrologic system.

Melesse and Graham (2004) proposed a grid based cell travel time hydrologic model that assumes invariant travel times during a storm event. The runoff hydrograph at the outlet of watershed is developed by routing the spatially distributed excess precipitation through the watershed using topographic data. Calculation of travel times from each cell to the watershed outlet requires computation of a runoff velocity for each grid cell. Velocity for each grid cell can be estimated depending on whether the grid cell represents an area of diffuse overland flow or more concentrated channel flow. This method ignores the variations in travel time during the storm because it takes average excess rainfall intensity. The advantage of Melesse and Graham's grid–based travel time method is that it can create a direct hydrograph without a spatially lumped unit hydrograph during a rainfall event.

The issue of invariant travel time proposed by Melesse and Graham (2004) is addressed by Du et al. (2009), who proposed a time variant spatially distributed direct

hydrograph travel time method (SDDH) to route spatially and temporally distributed surface runoff to the watershed outlet. In the time variant SDDH method, the cumulative direct runoff and travel time are calculated by summing the individual volumetric flow rates and travel times from all contributing cells to outlet along a flow path for a given time step. This approach, however, cannot maintain the total mass balance because a cell that receives input from multiple upstream cells gets accounted multiple times while computing the flow from upstream cells. Similarly a particular cell does not account for flow from adjacent cells while the flow is being routed from an upstream cell. For example, in Fig. 3.1, water from cell A flows to the outlet cell H through cells D–E–H. Similarly, water from cell B reaches the outlet through D–E–H. So if the flow at the outlet from cells A and B is computed as cumulative flow along the flow path, flows from D, E and H are accounted twice, thus compromising the mass balance. As a result, this technique requires adjustment of travel time (which is mistakenly referred to as calibration) to account for high volumetric flow rates computed through repeated accumulations. To overcome these issues in grid based hydrologic models based on travel–time concept, this study proposes a simple conceptual approach for distributed event based hydrologic modeling using the storage release approach.

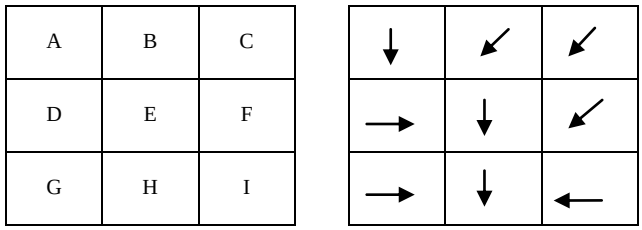

(a) Cell Identifier (b) Flow Direction

Figure 3.1 Example calculation in SDDH model.

3.3. Study Area and Data

The methodology for the STORE DHM is evaluated by applying it to multiple storm events at three study areas including Cedar Creek, Crooked Creek and Fish Creek in Indiana. A description of the study sites including their total area, land use type, elevations and annual precipitation is provided in Table 3.1, and their geographical locations are shown in Fig. 3.1. The three watersheds included in this study provide good test cases with respect to size and land use types. The geospatial data used in this study include: (i) topographic information in the form of a DEM from the United States Geological Survey (USGS); (ii) the 2001 National Land Cover Dataset (NLCD) also available from the USGS; and (iii) SSURGO soil data available from the National Resources Conservation Service (NRCS). Topographic attributes of each watershed such as flow direction, flow length, and slope are extracted from the DEM. The land use grid is used to compute Manning's n for velocity calculations, and to extract SCS curve numbers. Initial values of Manning's n for different land use types for all three study sites are presented in Table 3.2. Computation of SCS curve number also requires information on hydrologic soil group, obtained from the SSURGO soil data, which define the proportionate extent of the component soils and their properties for each map unit.

For each study site, hourly gauged rainfall data are obtained from the National Climatic Data Center, and NEXRAD *StageIII* radar rainfall data are obtained from the Ohio River Forecast Center (OHRFC). The NEXRAD rainfall dataset from OHRFC is distributed using the Hydrologic Rainfall Analysis Project (HRAP) projection. The HRAP or secant polar stereographic projection is an earth–centered datum coordinate system. Reed and Maidment (1995, 1999) describe the HRAP projection and its transformations to other geodetic coordinate systems. The NEXRAD *StageIII* data are converted to raster grids by using the methodology of Xie et al. (2005), which involves the following steps: (i) conversion of XMRG (binary) file format to ASCII; (ii) conversion of ASCII data to GIS grid format by first defining the HRAP projection, and then re–projecting it to a desired coordinate system; and (iii) clipping the rainfall grid over the area of interest. The computer programs needed to complete these steps are

available from the National Weather Service's office of hydrology web site (HTTP://WWW.NWS.NOAA.GOV/OH/HRL/DMIP/ NEXRAD.HTML).

The streamflow data for the study sites are obtained from the USGS Instantaneous Data Archive web site (HTTP://IDA.WATER.USGS.GOV/IDA/). The streamflow values from USGS include both base flow and surface runoff. In this study, the straight line base flow separation method is used for retrieving surface runoff hydrographs from streamflow.

Table 3.1 Study sites details for the STORE DHM Application.

Watershed	Area (km^2)	Land use	Elevation Range (m)	Average Slope (%)	Annual Precipitation (mm)
Cedar Creek	707	Agricultural (76%); forest (21%); urban (3%)	238 – 324	3	1100
Fish Creek	96	Agricultural (82%); urban (9%)	268 – 324	3.2	900
Crooked Creek	46	Urban (88%); agricultural (6%); forest (6%)	217 – 277	1.2	880

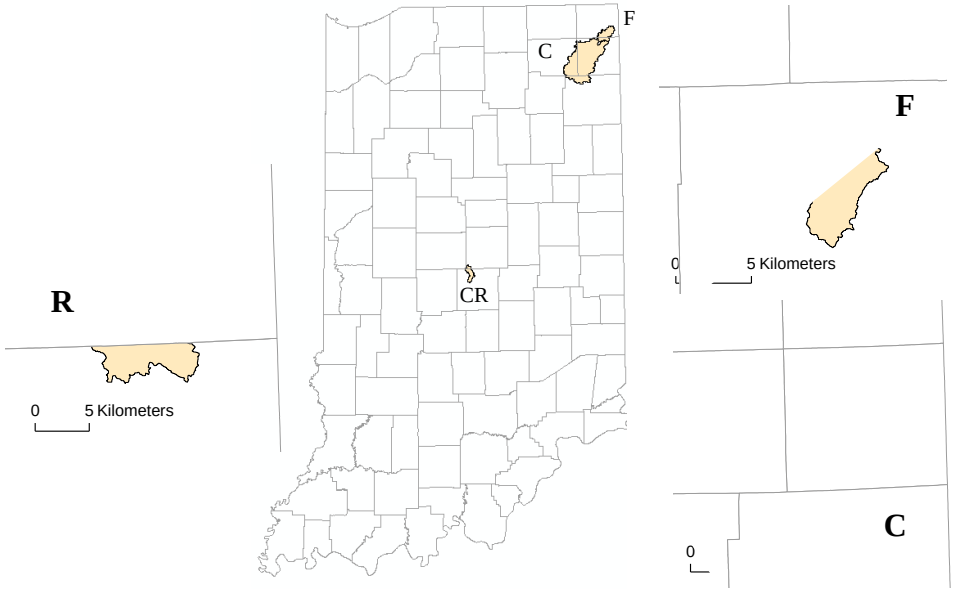

Figure 3.2 Study Areas for the STORE DHM Application (C – Cedar Creek, F – Fish Creek, R – Crooked Creek).

Table 3.2 Initial values of Manning's n.

Land use	Range	Initial Value
Agricultural	0.030–0.500	0.220
Forest	0.035–0.160	0.110
Developed	0.011–0.035	0.035
Water	0.025–0.033	0.033

3.4. Model Development

As mentioned in the Introduction section, the hydrologic model proposed here is a part of a broader modeling framework using object oriented concepts in GIS. In a nutshell, this object oriented framework uses a DEM as a hydrologic object that has properties and methods such as ComuteRunoff and RouteFlow to perform hydrologic simulations. The algorithm presented in this paper includes one set of methods that this grid based hydrologic object can implement. The object can be extended to implement additional methods including the ones from existing grid based models. The details of this object oriented framework are beyond the scope of Chapter 3, and only the conceptual framework behind the hydrologic modeling algorithm (STORE DHM) is presented.

3.4.1. Conceptual Framework

The conceptual framework for the STORE DHM involves computing excess rainfall, volumetric flow rate, and travel time to the basin outlet by combining steady state uniform flow approximation with Manning's equation. Basic elements of this conceptual framework are presented below followed by an example demonstration using Fig. 3.3.

A	B	C
D	E	F
G	H	I
J	K	L

Cell Identifier

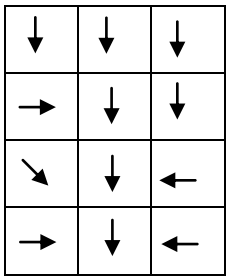

Flow Direction

0.10	0.10	0.10
0.10	0.10	0.10
0.10	0.10	0.10
0.08	0.08	0.08

Manning's n

21	13	09
12	09	06
06	03	02
03	03	02

Slope (%)

(a)

0.66	0.66	0.45
0.45	0.61	0.66
0.61	0.66	0.45
0.45	0.66	0.76

Pe_1 (mm/hr)

2.93	2.93	2.01
2.01	2.72	2.93
2.72	2.93	2.01
2.01	2.93	3.36

Q_1 (m^3/s)

0	0	0
0	0	0
0	0	0
0	0	0

R_1 (m^3/s)

10540	10540	7242
7242	9789	10540
9789	10540	7242
7242	10540	12089

S_1 (m^3)

8.1	9.4	12.4
11.2	11.1	11.9
19.4	14.3	18.2
14.8	13.0	13.7

T_1 (hr)

(b)

2.58	2.58	2.30
2.30	2.52	2.58
2.52	2.58	2.30
2.30	2.58	2.68

Pe_2 (mm)

11.45	11.45	10.22
10.22	11.21	11.45
11.21	11.45	10.22
10.22	11.45	11.92

Q_2 (m^3/s)

0.36	0.31	0.16
0.18	0.24	0.25
0.14	0.20	0.11
0.14	0.22	0.25

R_2 (m^3/s)

50481	50660	43457
44689	51045	51475
49627	52313	44532
43551	53578	54108

S_2 (m^3)

4.4	5.0	6.0
5.4	5.9	6.3
10.1	7.5	8.8
7.2	6.8	7.5

T_2 (hr)

(c)

Sample calculation for Sto_2 for cell *E*:

$Q_{E,2} = ie_{E,2}$ * Area = (2.52/3600) * 0.001 * (4000 ^2) = 11.20 m^3/s

$R_{E,2} = S_{E,1} * (\Delta T / t_{E,1}) = 2.72 * ((60*60)/(11.1147*3600)) = 0.24\ m^3/s$

$S_{E,2} = Q_{E,2}\Delta T + S_{E,1} - R_{E,2}\Delta T + R_{D,2}\Delta T + R_{B,2}\Delta T$ = (11.21*3600)+9789–(0.24*3600)+((0.18+0.31) *3600) = 51045 m^3

$V_{E,2} = (S_{E,2}/\Delta T) / (L*Y)$ = (51045/3600)/(4000*0.01834) = 0.19 *m/s*

$T_{E,2} = L/V_{E,2}$ = (4000)/ 0.19 = 21052 *s* = 5.85 *hr*

Figure 3.3 Sample calculations using a 3 x 4 hypothetical grid.

(1) Excess Rainfall

The main input to the model is rainfall that can come from either rain gauge(s) or radar (NEXRAD) data. The first step is to compute the excess rainfall by accounting for infiltration losses and depression storage. Excess rainfall is estimated by using the Soil Conservation Service (SCS) curve number technique (Eq. 3.1) for unsteady rainfall (SCS 1985). The excess rainfall (P_e in *mm*) is the portion of rainfall that remains after initial and continuous abstractions.

$$P_e = P - I_a - F_a \qquad \text{Eq. 3.1}$$

where P is precipitation (*mm*), and I_a = initial abstraction which is equal to 0.2*S_r. S_r is maximum soil water retention parameter (*mm*) given by Eq. 3.2, and F_a is the cumulative distribution of abstractions (*mm*) given by Eq. 3.3.

$$S_r = \frac{25400}{CN} - 254 \qquad \text{Eq. 3.2}$$

where CN = curve number.

$$F_a = \frac{S_r(P - I_a)}{P - I_a + S_r} \qquad P \geq I_a \qquad \text{Eq. 3.3}$$

The SCS curve number (CN) indicates the runoff potential of an area with a given combination of land use characteristics and hydrologic soil group.

(2) Excess Runoff

For a shallow water depth in overland or channel flow, the wetted perimeter is practically independent of the surface area, and the flow in each cell can be computed by Eq. 3.4 after Gupta et al. (1995).

$$Q_{i,t} = i_{e(i,t)} A \qquad \text{Eq. 3.4}$$

where $Q_{i,t}$ is the flow (m^3/s) corresponding to excess rainfall intensity $i_{e(i,t)}$ (equal to $P_{e(i,t)} / \Delta t^*$: Δt^* is time interval of rainfall) for a given time step (t) at the i^{th} cell, and A is the surface area (m^2) of the cell.

(3) Flowrate and Routing

After $Q_{i,t}$ is computed using Eq. 3.4, the flow is then routed by using a simple storage release approach. In this approach (Fig. 3.4), water within a watershed or stream can be assumed to flow through a series of buckets. At any given time step, each bucket stores the accumulated water of all upstream buckets that drain into it, and then releases the stored water to its next downstream bucket at the next time step as shown in Fig. 3.4. Following the conceptual model from Fig. 3.4, storage at any given time in any given bucket (or a raster cell in the context of this paper) is given by Eq. 3.5.

$$S_{i,t} = Q_{i,t}\Delta t + S_{i,t-1} - R_{i,t}\Delta t + \sum R_{u,t}\Delta t \qquad \text{Eq. 3.5}$$

where $R_{i,t}$ (given by Eq. 3.5) represents the release term from cell i in the t^{th} time step, and the difference between S and R represents the storage in the cell. The subscript u in Eq. 3.5 represents the surrounding upstream cells that are draining to cell i. In Fig. 3.4, each bucket or cell releases its stored water to a downstream cell depending on the residence or travel time of the water within each cell. The release term in Eq. 3.5 for each is computed by using Eq. 3.6.

$$R_{i,t} = \begin{cases} \dfrac{S_{i,t-1}}{\Delta t} & \text{if } T_{i,t-1} < \Delta t \\ \dfrac{S_{i,t-1}}{\Delta t} \times \left(\dfrac{\Delta t}{T_{i,t-1}} \right) & \text{if } T_{i,t-1} > \Delta t \end{cases} \qquad \text{Eq. 3.6}$$

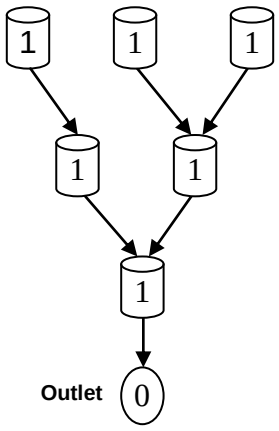	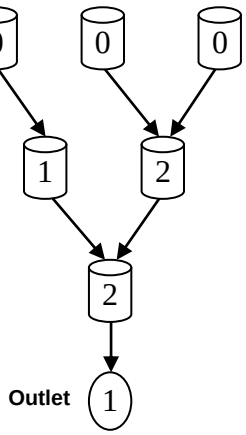	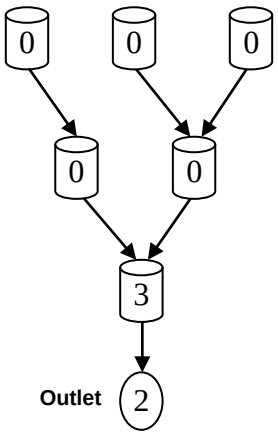
$^{\triangle}$t, all buckets are storing 1 unit of water with Q=0 at the outlet.	2$^{\triangle}$t, all buckets release their stored water to the next bucket and store water from upstream buckets. There is no additional input.	3$^{\triangle}$t, storage from upstream, and release to downstream continues.

Figure 3.4 Storage release concept.

where $T_{i,t}$ is the travel time within each cell, and is estimated depending on the flow conditions (overland flow or channel flow). In Eq. 3.6, all the water stored within a cell is released downstream if the travel time ($T_{i,t}$) is smaller than the model time step (Δt), or a fraction ($\Delta t / T_{i,t}$) of the water is released if the travel time is greater than the model time step.

(a) Travel time for overland flow

Overland flow travel time in a grid cell can be estimated by combining the steady state uniform flow approximation with Manning's equation (Singh and Aravamuthan, 1996). The overland flux can be given by Eq. 3.7 as shown below.

$$f^*_{i,t} = \frac{S_{i,t}}{\Delta t \cdot A} \qquad \text{Eq. 3.7}$$

where $f^*_{i,t}$ is the overland flow flux (*m/s*), and *A* is the surface area of the cell (m^2). The surface flow rate is calculated by using the Manning's equation below (Chow et al., 1988).

$$V = \frac{s_f^{1/2} y^{2/3}}{n} \qquad \text{Eq. 3.8}$$

where *V* = velocity (*m/s*), *y* is the depth of water on the surface (*m*), s_f is the friction slope and *n* is Manning's roughness coefficient. For steady state overland flow, unit width discharge in any given cell is:

$$q_{i,t} = f_{i,t}^* \cdot L_i = y_{i,t} V_{i,t} \qquad \text{Eq. 3.9}$$

where q is unit width discharge (m^2/s) and L is the flow length (equal to cell size for north–south and east–west flow, and equal to 1.414 times cell size for diagonal flow directions). Equation 3.9 can be written in terms of y as shown below.

$$y = \frac{f_{i,t}^{*} L_i}{V_{i,t}} \qquad \text{Eq. 3.10}$$

Equations 3.8 and 3.10 can be combined to get the following equation for V in each cell

$$V_{i,t} = \frac{s_i^{0.3} L_i^{0.4} f_{i,t}^{*\,0.4}}{n_i^{0.6}} \qquad \text{Eq. 3.11}$$

where $V_{i,t}$ is overland flow velocity (m/s) in i^{th} cell at time t and s_i is slope of surface in cell i. Travel time for any cell i is then computed from overland flow velocity and the flow distance using Eq. 3.12 below.

$$T_{i,t} = \frac{L_i}{V_{i,t}} \qquad \text{Eq. 3.12}$$

(b) Travel time for channel flow

Channel flow velocity, $V_{i,t}$, is computed by using Manning's equation and the continuity equation for a wide channel (Muzik, 1996; Melesse, 2002):

$$\frac{S_{i,t}}{\Delta t} = A_c V_t = B y_t V_t \qquad \text{Eq. 3.13}$$

where A_c is channel cross-section area.

$$y_t = \frac{S_{i,t}}{BV_t \Delta t} \qquad \text{Eq. 3.14}$$

where B is channel width (m). Manning's equation for channel flow is:

$$V = \frac{s_f^{1/2} R^{2/3}}{n} \qquad \text{Eq. 3.15}$$

where R is the hydraulic radius (cross–sectional area divided by wetted perimeter). For a wide channel $R = y$, and assuming $s_f = s_i$, Eqs. 3.14 and 3.15 yield

$$V_{i,t} = \left[\frac{s_i^{0.5}}{n_i} \left(\frac{S_{i,t}}{B\Delta t} \right)^{0.67} \right]^{0.6} \qquad \text{Eq. 3.16}$$

Travel time for any cell i is then computed from channel flow velocity and the flow distance.

$$T_{i,t} = \frac{L_i}{V_{i,t}} \qquad \text{Eq. 3.17}$$

Computation of S_i and R_i can be explained by considering a hypothetical grid shown in Fig. 3.1. Figure 3.1 (a) shows the flow direction, Manning's n and slope for each cell in the model domain. Figures 3.1 (b) and 3.1 (c) show Q_i, S_i, T_i and R_i for each cell due to excess rainfall (P_e) in two time steps (t=1 and 2). In Fig. 3.1 (b), $S_{i,t} = Q_{i,t}$ for the first time step (t = 1) because $R_{i,t}$, $R_{u,t}$ and $S_{i,0}$ have zero values. $T_{i,t}$ corresponding to $S_{i,t}$ is computed by using Eq. 3.12 or 3.17. For the next time step (t = 2 and t = 60 min), sample calculations for cell E are presented at the bottom of Fig. 3.1. The release term ($R_{i,t}$) at the outlet cell (K) produces the surface runoff hydrograph for the watershed.

(3) Selection of Model Time Step (Δt)

In any grid based model such as the STORE DHM presented in Chapter 3, the grid size affects the estimation of topographic parameters like slope, flow direction and flow path, thereby affecting the travel time computation, and eventually the flow hydrograph. As a result, a model that works at one given DEM resolution may not work for other DEM resolutions. Specifically, a finer resolution DEM produces lower peak (larger travel time), and a coarser resolution produces higher peak. Thus the model time step should be selected to ensure consistency in model results for different resolution DEMs. For any given DEM resolution, there is a minimum time step at which the water in all cells in a DEM will move to the next downstream cell. This time step is referred in this paper as the critical cell travel time (CCT). The CCT depends largely on DEM resolution, but is also affected by surface roughness, watershed slope and rainfall intensity. Estimation of CCT (in seconds using Eq. 3.18) for a given DEM resolution is based on the minimum surface roughness (n) and maximum slope (S) among all grid cells, and the flow (Q in m^3/s) corresponding to the maximum rainfall intensity in the watershed.

$$CCT = \frac{L}{Q / \ [(n \cdot Q) / (s^{0.5} \cdot L)]^{0.6} \cdot L} \qquad \text{Eq. 3.18}$$

where CCT is in seconds and L is cell size in meters. CCT values for Cedar Creek DEM for different resolutions are presented in Table 3.3, and the effect of CCT in selecting the model time step for the STORE DHM simulations is presented in Fig. 3.5 using five different (30m, 150m, 300m, 500m and 1000m) DEM resolutions. Fig. 3.5 (a) shows the output from the STORE DHM for different grid resolutions using 15 min. model time step, and as expected the peak increases with cell size. However, if the model simulation time step is less than CCT for each DEM resolution, the output hydrographs are consistent (Fig. 3.5 (b)). Thus, all simulations in this study are conducted using a time step smaller than CCT to account for the effect of DEM size on model results.

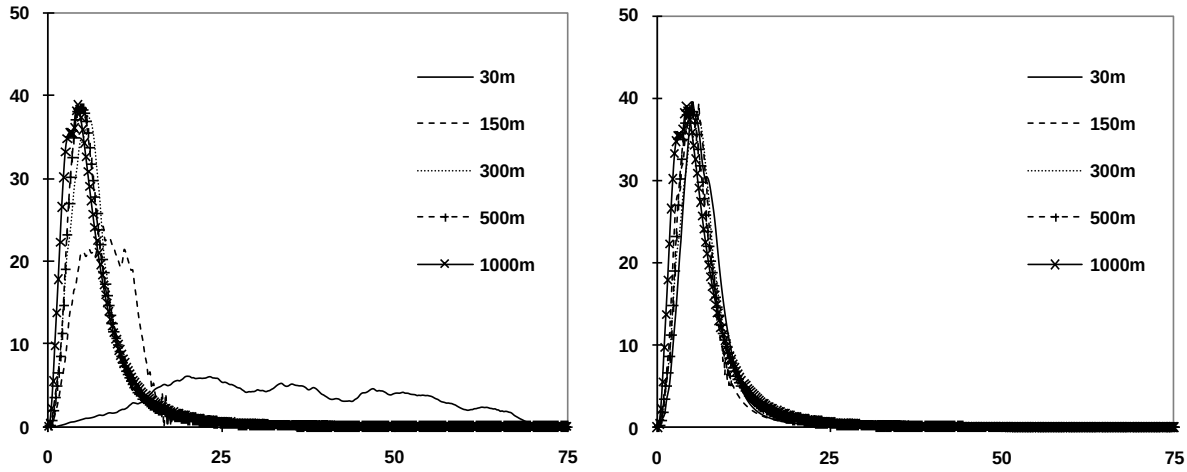

Figure 3.5 Cedar Creek model hydrographs with different DEM resolutions: (a) STORE DHM simulation with 15min simulation time step: (b) STORE DHM simulation using time step based on CCT.

Table 3.3 CCT for different grid resolutions using Cedar Creek DEM

DEM size(m)	CCT (hr)	CCT (min)
30	0.076	4.56
150	0.199	11.94
300	0.301	18.06
500	0.409	24.54
1000	0.621	37.26

3.5. Results

3.5.1. Model Calibration and Verification

Four isolated storms are selected for model application at the three study sites (details presented in Table 3.4), and the model output is validated against observed streamflow data at a USGS gauging station located at the outlet of each study site. The model is executed by using both gauged and NEXRAD data, and the results are evaluated by using two performance measures: the Nash Sutcliffe efficiency coefficient (E_{NS}) given by Eq. 3.19 (Nash and Sutcliffe, 1970), and the co–efficient of determination (R^2).

$$E_{NS} = 1 - \frac{\sum_{i=1}^{n} (X_{oi} - X_{si})^2}{\sum_{i=1}^{n} (X_{oi} - \overline{X_{oi}})^2} \qquad \text{Eq. 3.19}$$

where $\overline{X_{oi}}$ = average measured value during the simulation period, X_{si} = simulated output on step i, and X_{oi} = observed data on step i.

Table 3.4 Details of storm events for each site.

Study Site	Event #	Start Date and Time	Time Step (hr)	Total Precipitation (mm)		Total Streamflow (mm)	Peak Flow (m^3/s)	Time to Peak (hr)
				Gauge	NEXRAD			
Cedar Creek	1	05–02–02, 00:00	1.00	7.68	8.49	4.79	23.36	30.0
	2	05–02–21, 01:00	1.00	9.46	8.86	6.32	27.30	26.0
	3	05–03–19, 16:00	0.50	8.89	8.94	2.88	12.80	17.5
	4	06–01–13, 22:00	0.25	17.10	16.99	3.91	24.95	14.5
Fish Creek	1	05–01–12, 22:30	0.50	40.34	34.74	12.58	8.67	25.0
	2	05–03–06, 13:30	0.50	11.39	14.71	3.37	2.10	28.5
	3	06–01–02, 16:00	0.50	15.24	17.47	5.33	3.03	20.5
	4	06–02–16, 08:30	0.50	20.39	21.17	4.64	3.34	27.0
Crooked Creek	1	05–01–03, 14:45	0.25	45.72	38.25	15.93	28.07	7.5
	2	05–01–11, 08:45	0.25	36.13	33.21	12.01	16.57	8.5
	3	05–02–05, 12:45	0.25	31.56	31.39	6.21	7.39	11.5
	4	05–02–13, 06:15	0.25	40.64	36.56	18.99	18.41	6.0

The STORE DHM is first executed without calibration for each study site using rain gauge data for event 1 (C1, F1 and R1 in Table 3.5). The resulting hydrographs and then properties are presented in Fig. 3.6 and Table 3.5. Un–calibrated results show that the peak flow is underestimated by 30% for Cedar Creek, overestimated by 30% for Fish Creek, and within less than 0.5% error for Crooked Creek. Similarly, the time–to–peak is overestimated for Cedar Creek (10%) and Crooked Creek (33%) and underestimated for Fish Creek (20%). Overall, the total run–off depth between the model output and observed data looks reasonable for both Fish and Crooked Creek, and for Cedar Creek, the model runoff is 20% lower than observed runoff. The Nash–Sutcliffe coefficient is lower than 0.7 for all simulations. After the un–calibrated simulation for event 1, the model is calibrated manually for the same event at each study site by treating Manning's n as the calibration parameter. Calibrated values of Manning's n for each land use at each study site are presented in Table 3.6.

Table 3.5 Uncalibrated models results for Event 1 at each study site (C is Cedar Creek, F is Fish Creek and R is Crooked Creek.).

Area	Runoff Depth (mm)	Peak Flow (m^3/s)	Time to Peak (hr)	R^2	E_{NS}
C1	3.915	16.340	33.0	0.72	0.57
F1	11.809	11.030	19.5	0.83	0.68
R1	14.889	27.080	10.0	0.65	0.63

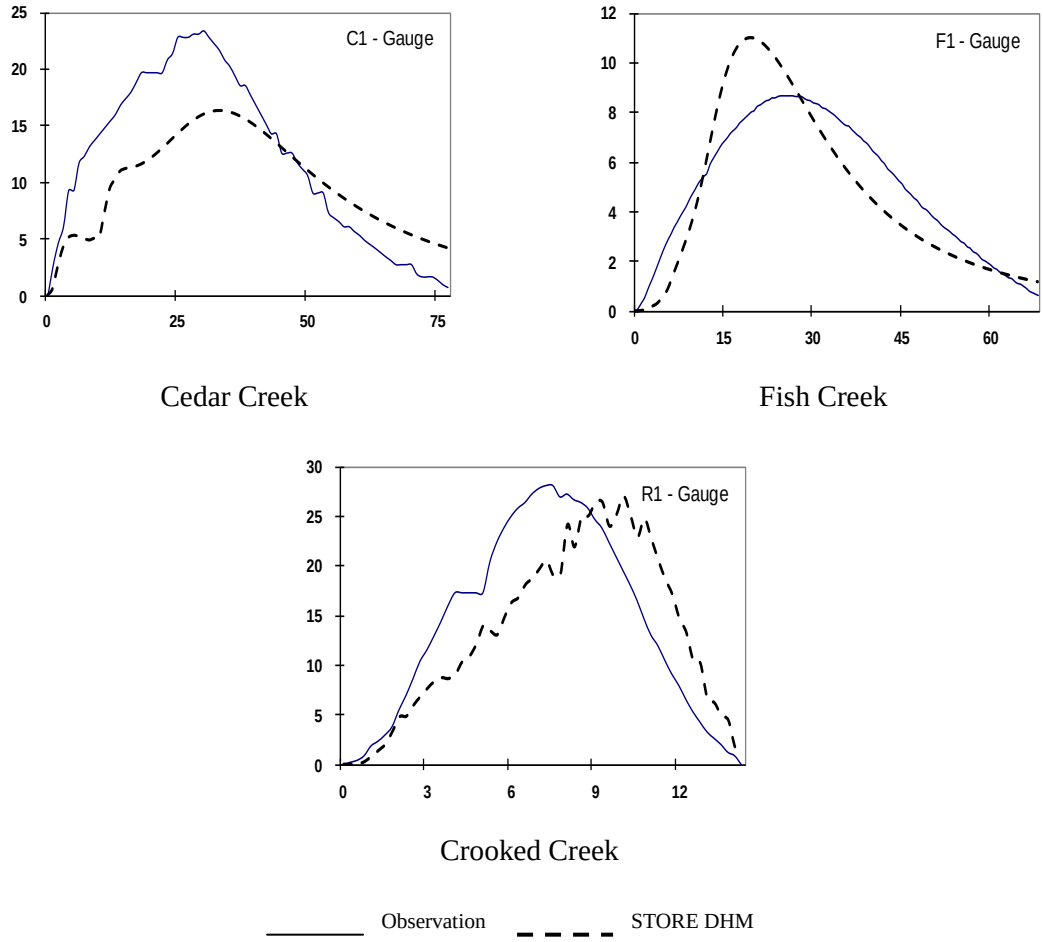

Figure 3.6 Uncalibrated model results for Event 1 (C1, F1 and R1) using gauged rainfall input. X–axis represents time in hours and Y–axis represents flow in cubic meters per second.

Table 3.6 Manning's n for study areas.

Land use	Range	Initial Value	After Calibration		
			Cedar Creek	Fish Creek	Crooked Creek
Agricultural	0.030–0.500	0.220	0.103	0.253	0.153
Forest	0.035–0.160	0.110	0.092	0.232	0.132
Developed	0.011–0.035	0.035	0.083	0.193	0.043
Water	0.025–0.033	0.033	0.006	0.076	0.026

Table 3.7 Calibration and validation results for all events (1–4) for Cedar Creek (c), Fish Creek (F) and Crooked Creek (R) using gauge rainfall.

Event	Simulation with Gauge Rainfall				
	Runoff Depth (mm)	Peak Flow (m^3/s)	Time to Peak (hr)	R^2	E_{NS}
C1	4.30	22.92	26.00	0.90	0.87
C2	6.03	36.00	26.00	0.92	0.78
C3	2.49	12.88	21.00	0.98	0.95
C4	3.08	23.89	14.50	0.95	0.85
F1	10.96	8.50	25.00	0.86	0.81
F2	2.93	1.97	14.00	0.89	0.82
F3	4.96	2.84	21.50	0.90	0.88
F4	5.05	3.29	29.00	0.90	0.87
R1	16.00	27.58	8.25	0.84	0.84
R2	10.95	17.12	9.75	0.91	0.89
R3	5.83	7.40	10.75	0.76	0.73
R4	15.15	19.87	7.25	0.91	0.87

Table 3.8 Calibration and validation results for all events (1–4) for Cedar Creek (c), Fish Creek (F) and Crooked Creek (R) using NEXRAD rainfall.

Event	Simulation with NEXRAD Rainfall				
	Runoff Depth (mm)	Peak Flow (m^3/s)	Time to Peak (hr)	R^2	E_{NS}
C1	4.65	23.36	27.00	0.88	0.88
C2	4.88	28.27	23.00	0.94	0.83
C3	2.57	13.18	21.50	0.97	0.95
C4	3.10	24.26	11.00	0.74	0.64
F1	10.44	8.07	23.50	0.91	0.81
F2	3.61	1.87	24.50	0.83	0.81
F3	5.24	3.21	13.50	0.93	0.93
F4	5.57	3.14	27.00	0.80	0.70
R1	15.77	28.60	7.25	0.97	0.97
R2	9.98	14.74	8.00	0.94	0.85
R3	5.83	7.00	11.50	0.75	0.74
R4	12.48	17.80	7.75	0.84	0.71

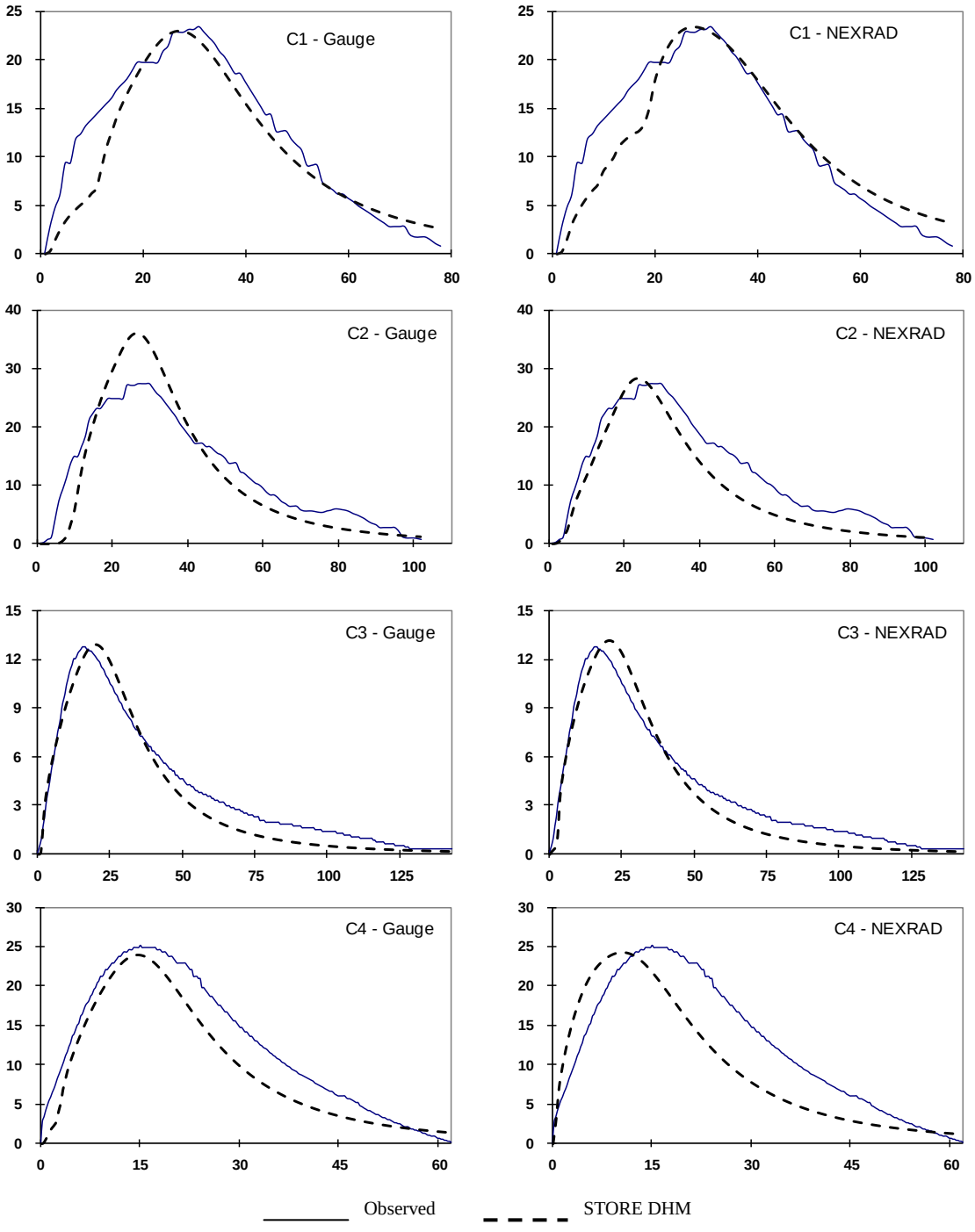

Figure 3.7 Cedar Creek model hydrographs. X–axis represents time in hours and Y–axis represents flow in cubic meters per second.

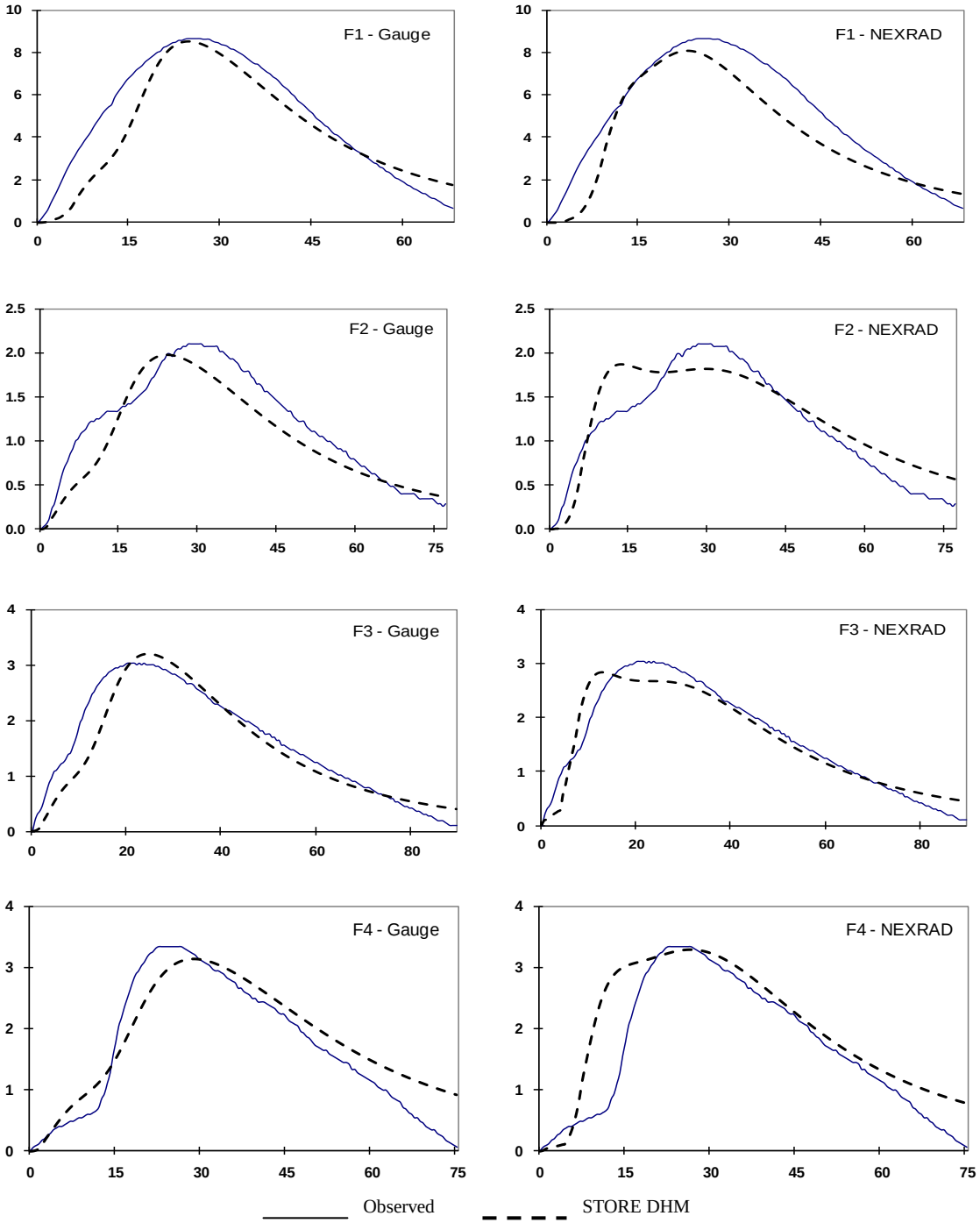

Figure 3.8 Fish Creek model hydrographs. X–axis represents time in hours and Y–axis represents flow in cubic meters per second.

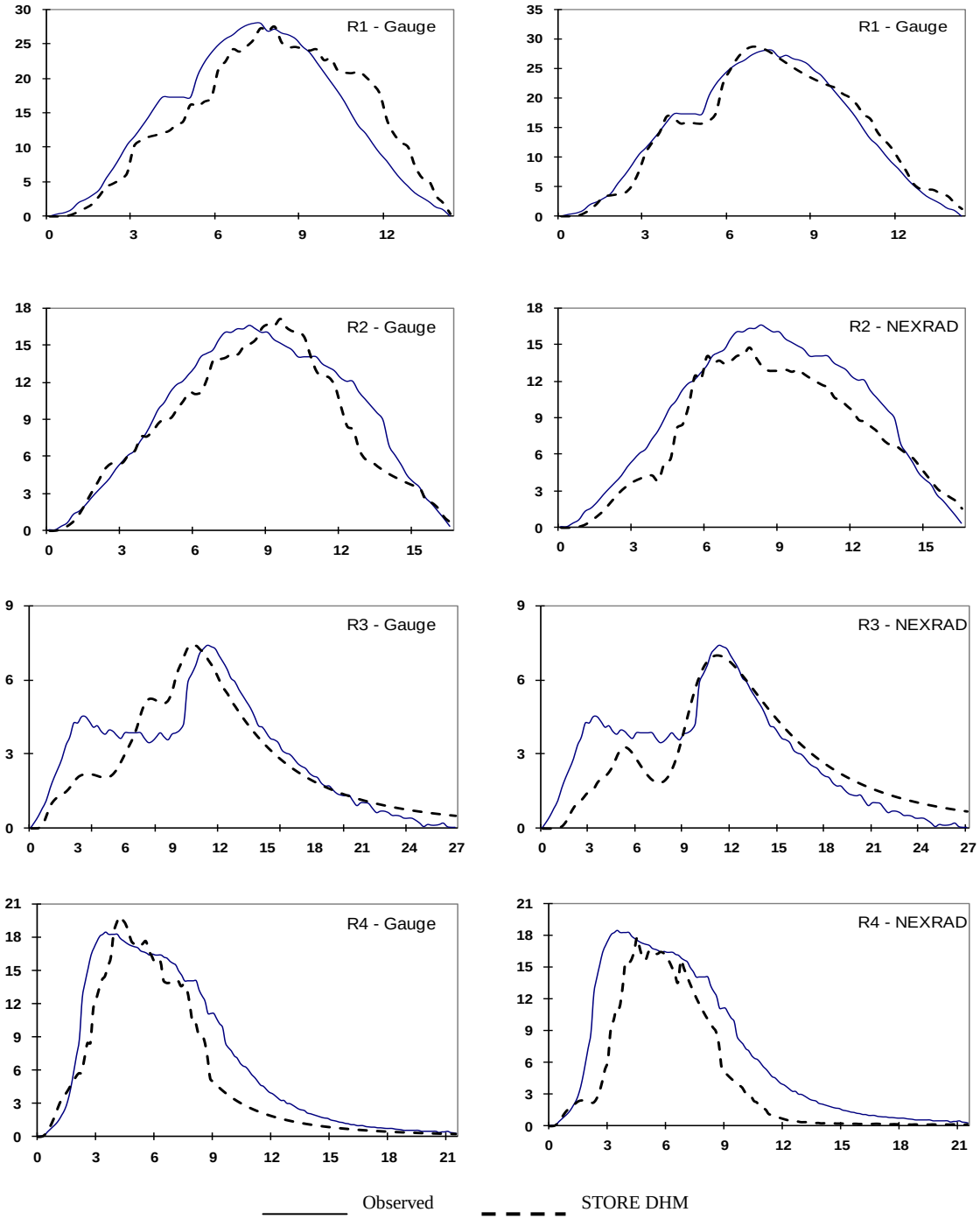

Figure 3.9 Crooked Creek model hydrographs. X–axis represents time in hours and Y–axis represents flow in cubic meters per second.

After calibration using gauged rainfall, the model is applied to the same event using NEXRAD input, and these results are presented in Tables 3.7 and 3.8. Tables 3.7 and 3.8 also present results from application of the model for three additional events at each site using both rain gauge and NEXRAD rainfall input. Hydrographs corresponding to results in Tables 3.7 and 3.8 are presented in Figs. 3.7–3.9 for each study site. Qualitative and quantitative comparisons of each model hydrograph (peak flow, total run–off depth and time–to–peak in Tables 3.7 and 3.8) with observed hydrograph show reasonable agreement (Table 3.4). Two performance measures (R^2 and E_{NS}) used in this study give a value of 0.8 or higher for most events included in this study with an average R^2 and E_{NS} of 0.88 for Cedar Creek, 0.85 for Fish Creek, and 0.85 for Crooked Creek. Regardless of the values of performance measures, the differences between observed data and model results including the differences between gauged and NEXRAD output can be attributed to the overall modeling approach and the quality of the input data.

3.5.2. Comparison with HEC–HMS

In addition to calibrating and validating the STORE DHM against independent storm events, the model results are compared with another event based model, HEC–HMS, for storm events in Cedar Creek. The HEC–HMS model for Cedar Creek also uses the SCS curve number method for computing excess rainfall, and the excess rainfall is transformed to the runoff hydrograph using the Clark Unit Hydrograph method. The routing through river channels is simulated by using the simple lag method. The Clark unit hydrograph method has two parameters (Time of Concentration and Storage Coefficient), and the lag method has one parameter (Lag time). Thus, the HEC–HMS simulations used in this study involve three parameters. Similar to STORE DHM, HEC–HMS is calibrated for these three parameters by using the data for the first storm event. The calibrated model is then validated by conducting simulations for three additional storm events in Cedar Creek. Table 3.9 presents a summary of model results and error

statistics for HEC–HMS simulations. Excluding the calibration results for event 1, HEC–HMS over estimates the peak discharge by 40% for Event 2 to more than 200% for event 3 (Fig. 3.10). The time–to–peak is underestimated for events 2 and 4, and overestimated for event 3. Results for events 3–4 are particularly discouraging from HEC–HMS in terms of the overall hydrograph shape and run–off volume.

Table 3.9 HEC–HMS model results for Cedar Creek.

Event	HEC– HMS Simulation with Gauged Rainfall				
	Runoff Depth (mm)	Peak Flow (m^3/s)	Time to Peak (hr)	R^2	E_{NS}
C1	4.49	22.86	24.00	0.94	0.92
C2	8.98	37.09	21.00	0.85	0.18
C3	17.60	37.04	16.50	0.86	–9.66
C4	51.24	62.61	21.25	0.05	–16.53

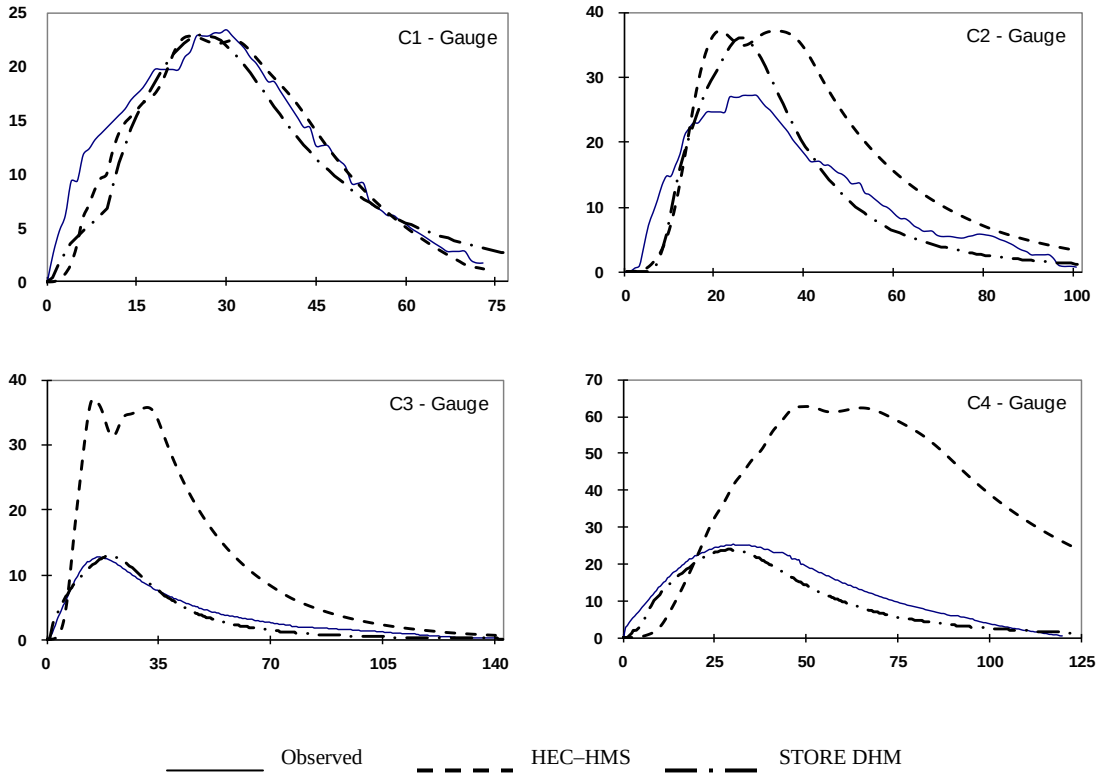

Figure 3.10 Comparison of HEC–HMS and STORE DHM hydrographs with observed data for Cedar Creek. X–axis represents time in hours and Y–axis represents flow in cubic meters per second.

3.5.3. Comparison with time variant SDDH Model

The results from the STORE DHM are compared with the grid based time variant spatially distributed direct hydrograph travel time method (SDDH) by Du et al. (2009). The methodology for this comparison is similar to that of HEC–HMS and involves calibration of the time variant SDDH model using the first storm event, and validation using the next three storm events. The velocity needed to compute the travel time in time variant SDDH is given by Eq. 3.20, which involves a parameter K that is determined through calibration. Through manual calibration of the model for Event 1, a value of 6.5 was determined for K, and used in subsequent simulations.

$$V = K s_0^{3/8} Q^{1/4} n^{-3/4} \qquad \text{Eq. 3.20}$$

where V is velocity in m/s, Q is discharge m^3/s, s_0 is the channel slope, and n is Manning's coefficient. Results (Fig. 3.11 and Table 3.10) show that time variant SDDH over estimates both peak discharge and time–to–peak for events 2–4 compared to the observed flow. The overestimation of peak discharge ranges from 15% for event 4 to 50% for event 2. Similarly, the time–to–peak is overestimated in the range of 10% for event 4 to 50% for event 2.

Table 3.10 Time variant SDDH model results for Cedar Creek.

Event	SDDH Simulation with Gauged Rainfall				
	Runoff Depth (mm)	Peak Flow (m_3/s)	Time to Peak (hr)	R^2	E_{NS}
C1	7.55	29.30	35.00	0.64	0.13
C2	10.16	44.54	32.00	0.86	–0.38
C3	8.21	20.48	26.00	0.82	–0.12
C4	28.06	30.30	15.75	0.84	0.74

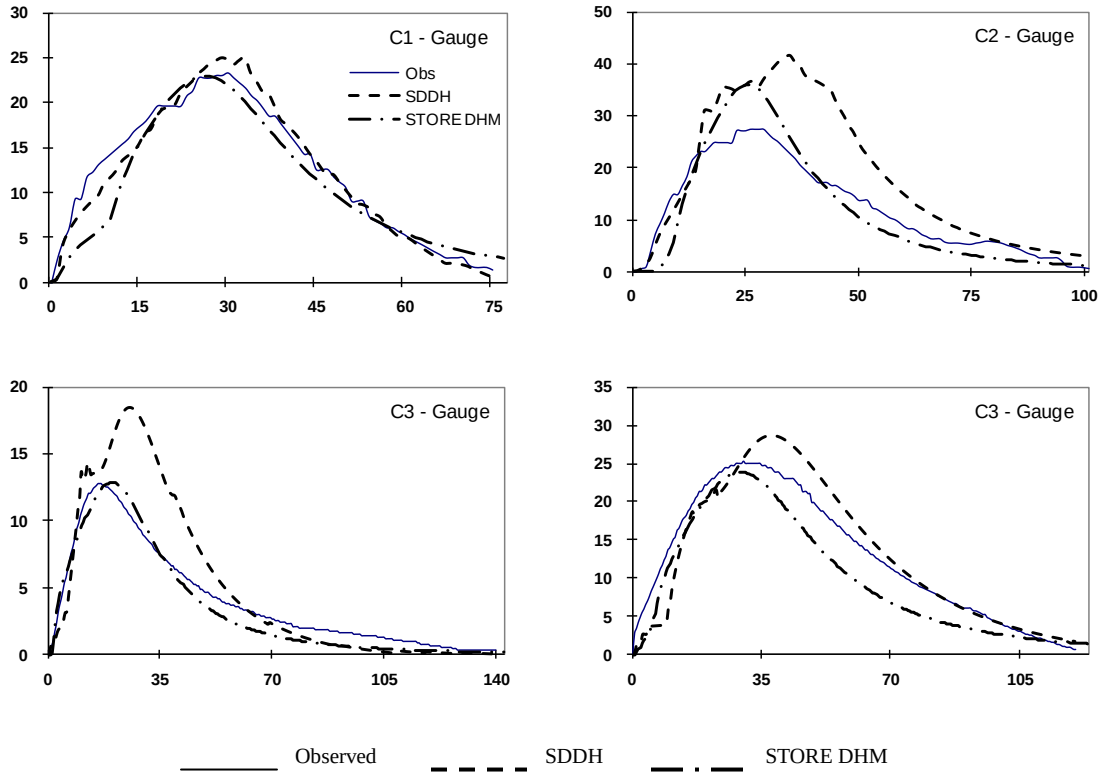

Figure 3.11 Comparison of time variant SDDH and STORE DHM hydrographs with observed data for Cedar Creek. X–axis represents time in hours and Y–axis represents flow in cubic meters per second.

3.6. Discussion

The storage release approach used in this study is dependent mainly on the travel time, which in turn is dependent on Manning's n. The fact that the model is calibrated using only one parameter is attractive from a practical point of view, but it sometimes becomes difficult to get both the peak flow and the time–to–peak to match with observed data. The error in peak flow for all simulations is much smaller compared to the error in time–to–peak. For example, the average percentage error in peak flow for Cedar Creek, Fish Creek and Crooked Creek is 7.8%, 4.2%, and 3.1%, respectively. The average percentage error in time–to–peak for Cedar Creek, Fish Creek and Crooked Creek is 8.0%, 28.8%, and 11.5%, respectively. Inclusion of more parameterized approaches for computing excess rainfall (or losses) such as the Green–Ampt Method may provide more flexibility in modeling hydrographs, but these options are still under development, and are not tested in this study.

Radar precipitation estimates are obtained by converting reflectance (Z) into precipitation (R) by using Z–R relationship (Smith, 1986). The Z–R relationship has uncertainties that affect the estimated radar precipitation, and in general, radar estimates tend to be different from rain gauge data. NEXRAD data attempts to reduce this difference by assimilating rain gauge data into radar precipitation estimate, but still some differences remain between rain gauge data and radar precipitation as evident from results in Table 3.4. For example in Crooked Creek watershed, which is mostly urban, total NEXRAD precipitation estimates are significantly lower compared to rain gauge data for three storm events (R1, R2 and R4); whereas for Fish Creek watershed (rural) NEXRAD precipitation estimates are higher than gauged data. Despite these differences in the input data, the overall model hydrograph shape is not different for both gauged and NEXRAD input (Figs. 3.7–3.9), but the total runoff depth (or volume) is different as shown in Tables 3.7 and 3.8.

The storage release approach in the STORE DHM does seem to capture the spatial distribution of rainfall as evident in C1 and C2 for Cedar Creek. In the case of C1, it seems that the rainfall was more uniformly distributed over the area thus giving

reasonable hydrographs for both gauged and NEXRAD. However for C2, higher rainfall recorded at the gauge yields higher runoff volume and peak (Fig. 3.7–C2), but the NEXRAD hydrograph matches well with observed data, thus suggesting that the rainfall observed at the gauge was higher than the average rainfall in the watershed. Similarly, the storage release approach seems to capture the bimodal nature of hydrographs observed in Crooked Creek watershed (Figs.3.9–R1 and 3.9–R3). The results with NEXRAD input are relatively better compared to gauged input for bimodal hydrographs. If it is assumed that NEXRAD precipitation provides better representation of the spatial distribution of rainfall in a watershed, then simulation results using Multisensor Precipitation Estimators (MPE) data should provide better output compared to the output from gauge rainfall in terms of peak flow and time–to–peak, which are important attributes in event based modeling. The results, however, show that output from MPE are not always better in terms of predicted peak flow and time–to–peak for some events compared to gauged data. These events include C4, F1, F2, F4, R1, R2 and R4 for peak flow as well as C2, C3, C4, F1, F3 and R4 for time to peak.

The inability of HEC–HMS to produce reasonable results for all Cedar Creek simulations (Fig. 3.10) is understandable considering that the hydrograph (C1) that was used for its calibration has different characteristics (e.g., shape, duration and flow peak) compared to the other three events (C2–C4) used for its verification. Similarly, although the output from time variant SDDH for Cedar Creek simulations is better compared to HEC–HMS, the peak flow is over estimated by time variant SDDH for all simulations. Comparison of STORE DHM with both HEC–HMS and time variant SDDH demonstrates its robustness in simulating different types of events with consistent results. This robustness of STORE DHM can be attributed to its dependence on only one parameter (Manning's n), which retains its physical meaning (representation of surface roughness) in all simulations, and the selection of model time step using the concept of critical cell travel time.

3.7. Conclusions and Future Work

The conceptual framework and application of a grid–based model, the STORE DHM, using the storage–release concept is presented in this study. Results show that the STORE DHM is able to simulate the hydrologic behavior of a watershed to produce streamflow hydrographs that match well with observed data. In addition, the STORE DHM is able to ingest both point and distributed rainfall input, and the comparison of outputs from these two types of inputs show that the storage–release approach is able to capture the rainfall dynamics in the NEXRAD data. Unlike other raster or grid–based models that route the flow from each cell to the watershed outlet along a common flow path at each time step (which can lead to improper water balance), the STORE DHM considers the flow contribution of neighboring cells by using the simple continuity equation (change in storage = input – output). This simplicity in turn provides computational efficiency, which is critical for real–time hydrologic forecasting. Similarly, the STORE DHM is a part of the broader GHISMO framework that provides flexibility in modular development of the model without changing the basic framework. For example, Chapter 4 presents a module to correct the bias (due to Z–R conversion and limited rain gauges information) in Multisensor Precipitation Estimator (MPE) NEXRAD data by developing an object for assimilating multiple data sources to get robust rainfall input.

The modeling framework presented in this chapter is operated within ArcGIS environment such that all the steps from extracting information from geospatial data to running model simulations are executed in ArcGIS environment. The approach from data to model output within a single environment is attractive from a practical point of view. Although the prototype modeling approach and its application including comparison with HEC–HMS and time variant SDDH is encouraging, there are several issues that still need to be addressed for this modeling framework to be fully useful for practical applications. These issues include: (i) testing the scalability of the model by applying it to larger watersheds (with more than 1,000 km^2 area) including regional basins (with areas in the range of several 10,000 km^2); (ii) investigation of computational efficiency and simplicity with multiple runoff generation mechanisms (e.g., Green–Ampt) and parameters; (iii)

ability of the model to ingest near real–time spatial (remote sensing) and temporal data for hydrologic modeling; and (iv) creating a protocol through which existing research codes can be converted to objects that can be incorporated into GHISMO.

CHAPTER 4. IMPROVING RAINFALL ACCURACY ON DISTRIBUTED HYDROLOGIC MODELING BY USING SPATIALLY UNIFORM AND NON–UNIFORM NEXRAD BIAS CORRECTION

4.1. Introduction

Representation of rainfall dynamics plays a critical role in making accurate hydrologic predictions. Numerous studies in the past decades have investigated the sensitivity of runoff hydrographs to rainfall by using gauged data. In addition to the accuracy of gauged rainfall input, the predictability and sensitivity of hydrologic models are dependent on the spatio–temporal representation of rainfall (Faures et al. 1995; Wilson et al. 1979; Troutman et al. 1989). To overcome these limitations, radar rainfall data are increasingly used in hydrologic applications (Smith et al., 2004). The next generation radar (NEXRAD) products available from 1992 provide high resolution rainfall information in space and time. Currently, the NEXRAD precipitation products are categorized into four levels according to the amount of preprocessing, calibration, and quality control performed. The *StageI* product is an hourly digital precipitation (HDP) directly derived from reflectivity measurements using a Z–R (reflectivity–rainfall) relationship after the application of several quality control algorithms (e.g. Fulton et al., 1998). *StageII* is the single radar site HDP product, which is merged with surface rain gauge observations to correct mean field bias using Kalman filtering (Smith and Krajewski, 1991; Anagnostou et al., 1999). In *StageIII*, the *StageII* rainfall data from multiple weather radars covering a River Forecast Center (RFC) region are combined (Fulton et al., 1998; Reed and Maidment, 1999). Finally, *StageIV* is the mosaicked *StageIII* rainfall product covering the entire Continental United States (CONUS).

The most commonly used NEXRAD product in hydrometeorological applications is the NEXRAD *StageIII* data (e.g. Young et al., 2000) since it involves the correction of radar rainfall rates with multiple surface rain gauges and has a significant degree of metrological quality control by trained personnel at individual RFCs (Fulton et al., 1998). Since around 2002, Multisensor Precipitation Estimator (MPE), which are developed by the National Weather Service (NWS) Office of Hydrology, is available for each RFC. The MPE product is obtained by merging radar, gauge and satellite estimates of rainfall and is adjusted for mean field and local biases. In spite of better spatial representation of rainfall variability by radar, there are limitations of radar estimates due to data contamination and uncertainty issues (Smith et al., 1996; Legates, 2000; Xie et al., 2006). In particular, uncertainty in radar rainfall is caused by reflectivity–rainfall conversion method, limitation of available rain gauge information for mean field bias adjustment and spatially uniform bias correction for entire RFCs. Minimizing errors in radar precipitation has been one of the major tasks in hydrologic and meteorologic research for decades (Schimid and Wuest, 2005).

An intense topic of water resources research has been merging radar and gauge rainfall to estimate a high accuracy rainfall. Smith and Krajewski (1991) found that combining radar and gauge information produces improved precipitation estimates, in terms of both quality and spatial resolution, in comparison with either radar or gauge estimates alone. Krajewski (1987), Pereira et al. (1998) and Seo (2002) proposed co–kriging, statistical objective analysis and Kalman filtering approach, respectively. However, uncertainty persists in radar precipitation products because large portions of radar coverage areas do not have rain gauge data to adjust biases in radar rainfall (Winchell et al., 1998; Habib et al., 2009). The different radar rainfall error correction schemes in mountainous areas are investigated by Dinku et al. (2002). Correction for terrain blocking, adjustment for rain attenuation, and interpolation of reflectivity data are used for radar rainfall error correction. They also used a Kalman filtering–based mean field radar bias correction scheme that is similar to the approach of the Anagnostou and

Krajewski (1998) study. They found that adjustment of radar bias with the filtering approach produced extremely high accuracy radar rainfall.

In NEXRAD *StageIII* (MPE), analysis bias in radar rainfall is corrected using available rain gauges. The correction procedures assume that the biases are spatially uniform over the entire RFC region. These spatially uniform biases are referred to as mean field bias (Smith and Krajewski, 1991). However, recent studies have shown that the assumption of spatially uniform bias is not valid over particular regions (Li et al., 2010). The NEXRAD rainfall bias over a small watershed in an RFC region could be very different from the mean bias over the entire RFC region. Looper et al. (2009) concluded that even though MPE already takes radar bias correction, the resulting precipitation may not be accurate for a particular river basin, because adjustment is performed on the entire RFC region. Consequently, hydrologic model simulations for a particular watershed with MPE analysis data could be unrealistic. Nevertheless, the effect of these spatially non–uniform local biases on hydrologic simulations is not well understood (Li et al., 2010). Further, the few methods that are available to correct spatially non–uniform local biases (Seo et al., 2001) have limitations such as limited number of rain gauge data for correcting local radar biases, and their sensitivity to hydrologic model simulations has not been tested.

Literature shows that the availability of high–resolution precipitation data from different weather radar platforms has led to improved understanding of rainfall uncertainty in hydrologic models, but few efforts have been directed towards understanding the influence of NEXRAD precipitation and its bias correction on rainfall–runoff simulations. This study presents three different NEXRAD rainfall bias correction schemes and their influence on sensitivity of grid based distributed hydrologic model simulations.

4.2. Study Areas and Data

The Upper Wabash River and the Upper Cumberland River (Fig. 4.1) basins are selected as the test beds for this study. In addition to providing two distinct geographic locations, both study areas include a reasonable rain gauge network to compare bias correction schemes using NEXRAD data. The Upper Wabash River basin (UWR; 17,907 km^2) is located in north central Indiana, and it drains into the Wabash River. The elevation in UWR ranges from 149 to 529 m. Normal annual precipitation of the UWR ranges between 920 and 1120 mm as computed by using data from 17 rain gauges in the region. The Upper Cumberland River basin (UCR; 38,160km^2) is located in southeastern Kentucky bordering with Virginia and Tennessee. The UCR is primarily mountainous and forested, and it lies in the Eastern Coal Field physiographic region. The elevation in the UCR ranges from 146 to 1428 m. Normal annual precipitation of the UCR ranges from 950 to 1300mm as computed from 19 rain gauges in the region.

The NEXRAD rainfall dataset for the study area is distributed by HRAP (Hydrologic Rainfall Analysis Project) geographic projection. The HRAP or secant polar stereographic projection is an earth–centered datum coordinate system. Reed and Maidment (1995, 1999) describe the HRAP projection and its transformations to other geodetic coordinate systems. The NEXRAD *StageIII* data are converted to re–projecting ASCII by using C++ program for conversion of XMRG (binary) file format to ASCII, and conversion of ASCII data to GIS grid format by first defining the HARP projection to the desired coordinate system. Rain gauge measurements of five storms recorded on February, April, July, October and November, 2006 for the UWR and January, February, March, April and July, 2005 for the UCR are selected for this study. The observational networks of NEXRAD *StageIII*, rain gauges, and stream gauges that cover the UWR and the UCR basins are shown in Fig. 4.2, and Table 4.1 displays summary of rainfall event for each site.

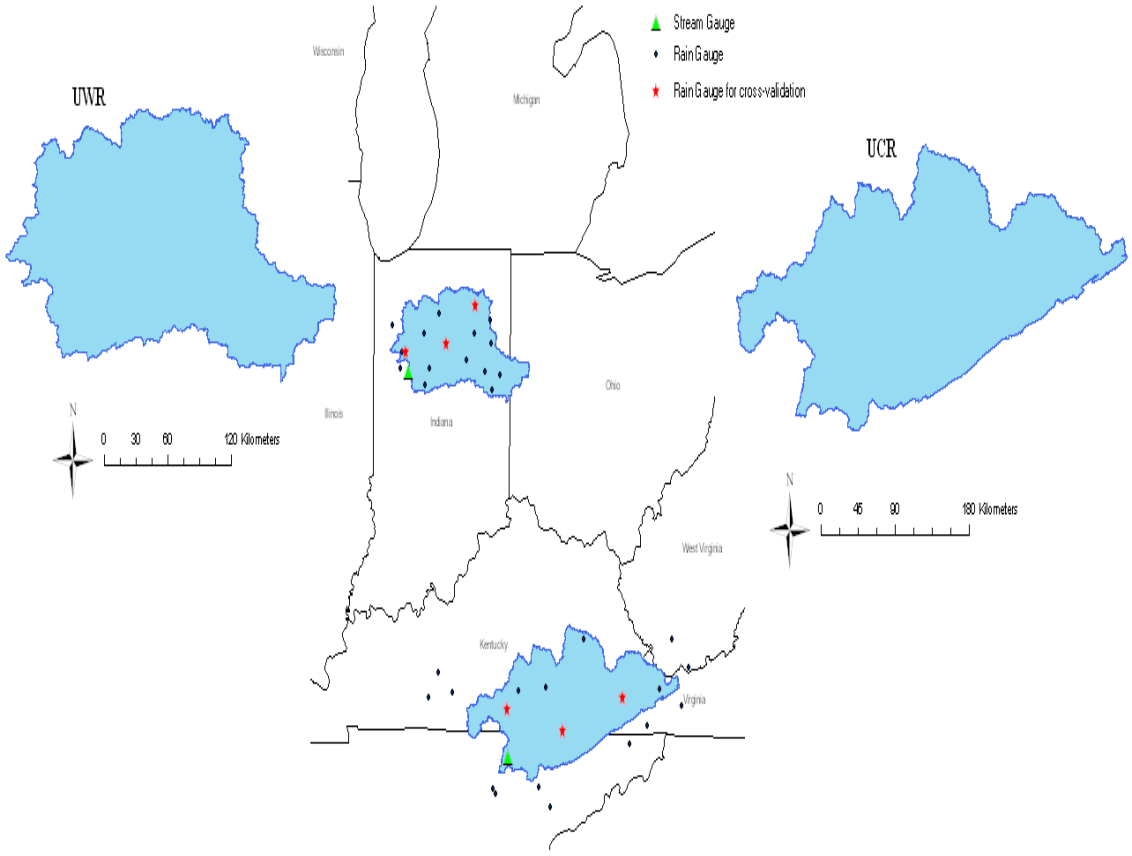

Figure 4.1 Study basin locations in relation to rain gauges and stream gauges (UWR – Upper Wabash River basin, UCR – Upper Cumberland River basin).

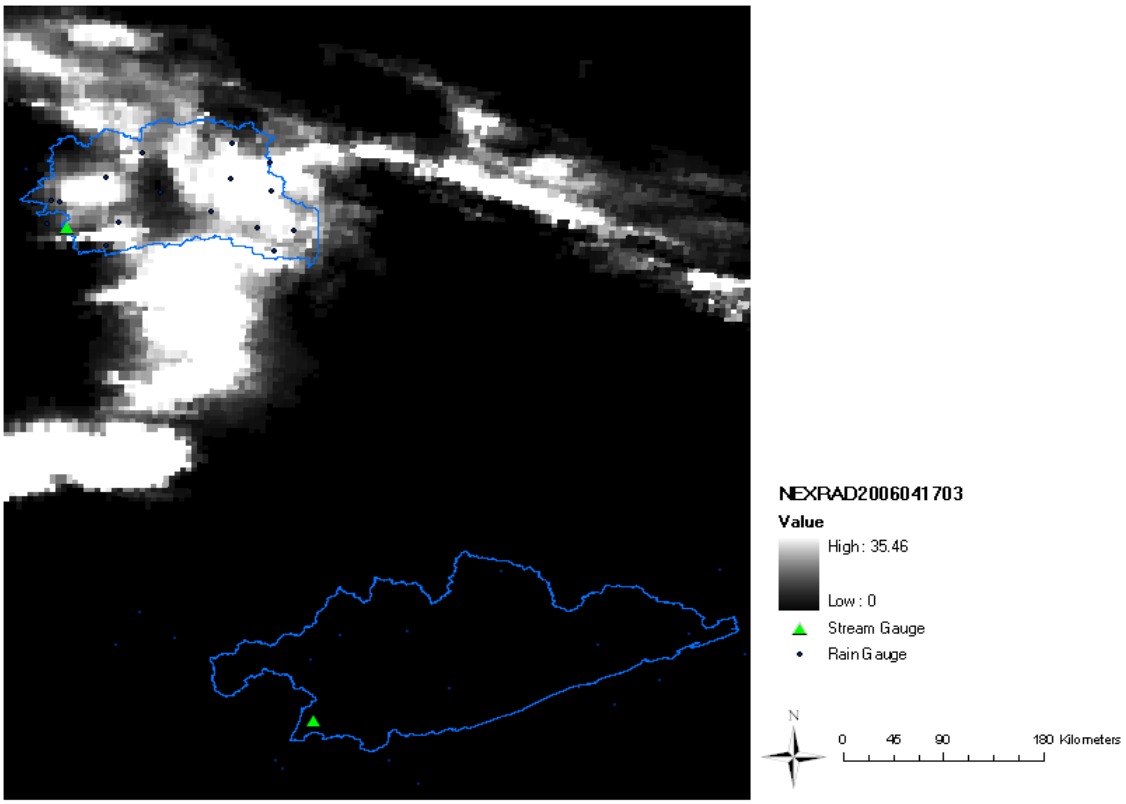

Figure 4.2 Basin locations and surrounding NEXRAD *StageIII*.

Table 4.1 Summary of storm events for application of NEXRAD bias correction.

Event	Upper Wabash River Basin	Upper Cumberland River Basin
	Start Date and Time	Start Date and Time
1	06–02–17, 01:00	05–01–11, 12:00
2	06–04–16, 19:00	05–02–13, 10:00
3	06–07–12, 03:00	05–03–27, 23:00
4	06–10–27, 19:00	05–04–01, 18:00
5	06–11–16, 08:00	05–07–13, 08:00

4.3. NEXRAD Bias Correction Methods

A statistical method should be used to remove the bias between NEXRAD estimates at the rain gauge locations, and corresponding gauge rainfall measurements because NEXRAD rainfall estimates have errors from reflectivity measurement and the Z–R conversion. To test the sensitivity of NEXRAD bias correction on runoff hydrographs, three methods based on the Kalman filter are used in this study. The first method is based on application of spatially uniform bias correction as used in MPE data. The second and third methods are based on the application of spatially non–uniform bias correction. A brief description of Kalman Filter and its application for spatially and non–spatially uniform bias correction is presented below.

4.3.1. Kalman filter

The Kalman filtering equations have two series of stages, which are *time update* and *measurement update*, to estimate the best possible bias. Projecting forward (in time) the current state is performed in *time update*. Correcting new *a priori* estimate at the current time step is performed in *measurement update* (Welch and Bishop, 2001).

(1) Discrete Kalman filter Time update

According to Smith and Krajewski (1991), NEXRAD bias (β) is assumed as an Autoregressive order one (AR1) process whose parameters are updated using a Kalman filter as given by Eq. 1.

$$\beta(t) = \rho_\beta \times \beta(t-1) + W(t);\ W(t) \sim \mathcal{N}(0, \nu) \qquad \text{Eq. 4.1}$$

where $\beta(t)$ is NEXRAD bias for hour *t*, ρ_β is lag–one correlation coefficient of the logarithmic bias, and *W(t)* is a sequence of independent normally distributed random variables with mean zero and variance ν. The stationary process variance (ν) and the stationary variance of the log bias process (σ_β^2) are given by Eqs. 4.2 and 4.3.

$$\nu = (1-\rho_\beta^2)\times\sigma_\beta^2 . \qquad \text{Eq. 4.2}$$

$$\sigma_\beta^2 = Var\ \beta(t)\ ; \text{t} = 0, \ldots, \text{T} \qquad \text{Eq. 4.3}$$

where T is storm duration.

The *a priori* estimate of β can be estimated using Eq. 4.4.

$$\bar{\beta}(t) = \rho_\beta \times \beta(t-1) \qquad \text{Eq. 4.4}$$

where β takes into account the new measurement that is observed, and corrects for any errors that may be present in the newly measured value.

The process variance ($P^-(t)$) is estimated using Eq. 4.5.

$$P^-(t) = \rho_\beta^2 \times P(t-1) + (1-\rho_\beta^2)\times\sigma_\beta^2 \qquad \text{Eq. 4.5}$$

where *P(t–1)* is the *a posteriori* estimate error variance at time *t–1*. The initial value of β_0 and P_0 are zero and σ_β^2, respectively.

(2) Discrete Kalman filter Measurement update

In each time and measurement update pair, the process is repeated with the previous *a posteriori* estimates used to project or predict the new *a priori* estimates. This

recursive nature is one of the important features of the Kalman filter. Updating the *a priori* estimates of the logarithmic NEXRAD bias $\beta^{-}(t)$ and the variance $P^{-}(t)$ based on the actual bias for the current time step *t* are calculated in *measurement update*. After this stage for time step *t*, the estimated logarithmic bias ($\beta(t)$) and its variance ($P(t)$) are calculated by Eqs. (9) and (10). The errors associated with the observed rain field lead to a deviation between the observed and true values for β_t. The observed logarithmic NEXRAD bias ($Y(t)$) is represented by using Eq. 4.6.

$$Y(t) = \beta(t) + M(t);\ M(t) \sim \mathcal{N}(0, \sigma\ \eta(t)^{\ 2}) \qquad \text{Eq. 4.6}$$

where $\sigma(\eta)$ is a nonnegative function representing the observation error given that the number of gauges with measurable rainfall is η, and $M(t)$ is a sequence of independent normally distributed random variable with mean zero and variance $\sigma(\eta)^2$. Estimations of $\beta(t)$ and $P(t)$ are used by $\sigma(\eta)^2$ which is suggested by Smith and Krajewski (1991).

$$\sigma(\eta)^2 = n^{-2} \qquad \text{Eq. 4.7}$$

where *n* is the number of the rain gauge.

The measurement update of the Kalman filter allows estimation of $\beta(t)$ and $P(t)$ by Kalman gain ($K(t)$) and it's detailed in Eqs. 4.8–4.10.

$$K(t) = P^{-}(t) \cdot (P^{-}(t) + \sigma(\eta)^2)^{-1} \qquad \text{Eq. 4.8}$$

$$\beta(t) = \beta^{-}(t) + K(t) \cdot (Y(t) - \beta^{-}(t)) \qquad \text{Eq. 4.9}$$

$$P(t) = (1 - K(t)) \times P^{-}(t) \qquad \text{Eq. 4.10}$$

Due to the bias model defined in terms of the log bias process, Smith and Krajewski (1991) suggest Eq. 4.11 for state expectation of the bias correction factor at the time *t* as shown below

$$B(t) = 10^{\left[\beta(t)+0.5P(t)\right]} . \qquad \text{Eq. 4.11}$$

4.3.2. Spatially uniform NEXRAD Bias Correction using Kalman filter

According to Seo et al. (1999) and Dinku et al. (2002), *mean field bias* corrections and *vertical profile of reflectivity* adjustments are needed to correct spatially uniform biases in NEXRAD data. The variance of the observed mean field bias should affect the magnitude of the Kalman filter observation error model. The time–dependent variance of the observed mean field bias (MFB) is estimated by using the variance of logarithmic bias proposed by Smith and Krajewski (1991). The correction procedures assume that the biases are spatially uniform over the entire study area. The logarithmic MFB between NEXRAD estimates at the rain gauge locations and the corresponding gauge rainfall amounts is computed by equation 4.12.

$$\beta(t) = \frac{\frac{1}{n}\sum_{i=1}^{n}\log_{10}(G(t)_i)}{\frac{1}{n}\sum_{i=1}^{n}\log_{10}(R(t)_i)} \qquad \text{Eq. 4.12}$$

where $G(t)_i$ is hourly rain gauge rainfall at NEXRAD–gauge paired cell *i* for hour *t*, $R(t)_i$ is hourly NEXRAD rainfall at NEXRAD–gauge paired cell *i* for hour *t*, and *n* is the number of radar–gauge pairs data available for an hour. The spatially uniform bias corrected NEXRAD rainfall is then computed by using Eq. 4.13.

$$R^*(t)_j = B(t) \cdot R(t)_j \qquad \text{Eq. 4.13}$$

where $R^*(t)_j$ is bias corrected NEXRAD at j location at time t, and $R(t)_j$ is hourly NEXRAD rainfall at gauge cell j for hour t within the study area.

4.3.3. Spatially non–uniform NEXRAD Bias Correction using Kalman Filter

In the spatially uniform bias correction method, the radar bias (Eq. 4.12) over the cells with observed rain gauge data is assumed to be uniform for all NEXRAD cells without corresponding rain gauges. The assumption of uniform bias may or may not be true depending on the rainfall dynamics and the size of the watershed. As a result, the bias may be higher for NEXRAD cells that do not overlap with rain gauge locations. In order to minimize such un–gauged NEXRAD cell bias, this study suggests application of a spatially non–uniform bias correction using Kalman filter. Unlike the MFB (Eq. 4.12), the spatially non–uniform biases vary from pixel to pixel across the NEXRAD domain. The corrected NEXRAD rainfall at an un–gauged NEXRAD pixel j for hour t, $R^*(t)_j$, is computed by multiplying spatially non–uniform bias correction factor ($B(t)_j$) at each un–gauged NEXRAD grid location j using Eq. 4.14.

$$R^*(t)_j = B(t)_j \cdot R(t)_j \qquad \text{Eq. 4.14}$$

There are two approaches for computing the spatially non–uniform bias. In the first approach, the rain gauge data are interpolated to get interpolated rainfall estimates for un–gauged NEXRAD pixels. The squared inverse distance weighting (IDW) method (Eq. 4.15) is used for interpolation. Compared with other methods like Kriging, even though

its method consists of simple approach, it provides flexibility enough to predict the variables with small size datasets in storm period (Adisoma and Hester, 1995).

$$G^*(t)_j = \frac{\sum_{i=1}^{n} w_i G(t)_i}{\sum_{i=1}^{n} w_i} \qquad \text{Eq. 4.15}$$

where $G^*(t)_j$ is interpolated gauge information at un–gauged NEXRAD pixel j for hour t, and w_i (Eq. 4.16) is the weight corresponding to each gauged point.

$$w_i = \frac{1/d_i^{\,b}}{\sum_{i=0}^{n} 1/d_i^{\,b}} \qquad \text{Eq. 4.16}$$

where d_i is the distance between a radar pixel and the i^{th} rain gauge, b is an empirical exponent and n is the number of rain gauges. The spatially non–uniform local NEXRAD biases can then be estimated and corrected by using the interpolated rainfall (Eq. 4.17).

$$\beta(t)_j = \frac{\log_{10}(G^*(t)_j)}{\log_{10}(R(t)_j)} \qquad \text{Eq. 4.17}$$

where $\beta(t)_j$ is logarithmic local bias at un–gauged NEXRAD pixel j for hour t within the study area.

In the second approach for applying non–uniform bias, the error at each gauged location is computed using Eq. 4.18.

$$e(t)_i = \frac{\log_{10}(G(t)_i)}{\log_{10}(R(t)_i)} \qquad \text{Eq. 4.18}$$

The errors at each i^{th} gauge are then interpolated to get errors at all ungauged NEXRAD pixels using squared inverse distance weighing. Ware (2005) found that the interpolation errors associated with this IDW are comparable to those obtained using the multi–quadric interpolation (Nuss and Titley, 1994) and ordinary kriging. An un–gauged NEXRAD bias for spatially non–uniform bias correction is computed based on surrounding ratios and distance of each gauge from the selected grid (Eq. 4.19).

$$\beta(t)_j = \frac{\sum_{i=1}^{n} w_i e(t)_i}{\sum_{i=1}^{n} w_i} \qquad \text{Eq. 4.19}$$

where $\beta(t)_j$ is logarithmic local bias at un–gauged NEXRAD pixel *j* for hour *t* within the study area.

4.4. Results

Results are presented in two sections. In the first section, the quality of NEXRAD data is assessed through cross–validation with observed rainfall. The NEXRAD data used in cross–validation is prepared by using the spatially uniform bias correction method (MPE), spatially non–uniform bias correction method by interpolating rainfall data (SNU–R), and spatially non–uniform bias correction method by interpolating errors (SNU–E). In the second section, the sensitivity of the STORE DHM hydrograph outputs to rainfall created by using spatially uniform and non–uniform bias correction is presented.

4.4.1. Assessment of NEXRAD Rainfall Inputs

The cross–validation of NEXRAD rainfall inputs created by using MPE, SNU–R and SNU–E is conducted by using a total 17 rain gauges in UWR and 19 rain gauges in UCR basins for five different events (Table 4.1). From the total number of gauging stations, three numbers are excluded for cross–validation. The scatter plot of NEXRAD bias corrected rainfall and cross–validated observed gauge rainfall for the UWR and the UCR are shown in Fig. 4.3. The results presents in Fig. 4.3 (a) and (b) indicate that the use of spatially uniform NEXRAD bias correction (MPE scheme) in estimating NEXRAD can increase scatter in comparison with spatially non–uniform NEXRAD bias correction. Considerable scatter is seen in the NEXRAD data created using the MPE scheme; whereas the data created using spatially non–uniform bias correction schemes show relatively low bias and error. The performance of bias corrected NEXRAD is assessed by computing the root mean square error (RMSE), mean absolute percentage error (MAPE) and coefficient of determination (R^2) as shown in Tables 4.2 and 4.3.

The spatially non–uniform NEXRAD bias correction improves rainfall accuracy in for the UWR events by reducing error from 1.17 RMSE mm for MPE to 0.80 mm RMSE for SNU–R and 0.94 mm RMSE for SNU–E. For the UCR events, the RMSE is reduced from 13.76 mm for MPE to 6.16 mm for SNU–R and 6.75 mm for SNU–R. The reduction in RMSE is more than –53% for the UCR, and more than –25% for the UWR by using spatially non–uniform bias correction method compared to the MPE scheme. Average values for MAPE also show similar results where the MAPE reduced by more than –59% for SNU–R and –45% for SNU–E compared to the MPE scheme. The average R^2 in the UWR (Table 4.2) is 0.67 for MPE scheme, 0.83 for SNU–R, and 0.76 for SNU–E. For the UCR dataset, the average R^2 is 0.30 for MPE scheme, 0.58 for SNU–R scheme, and 0.64 in SNU–E scheme (Table 4.3).

(a)

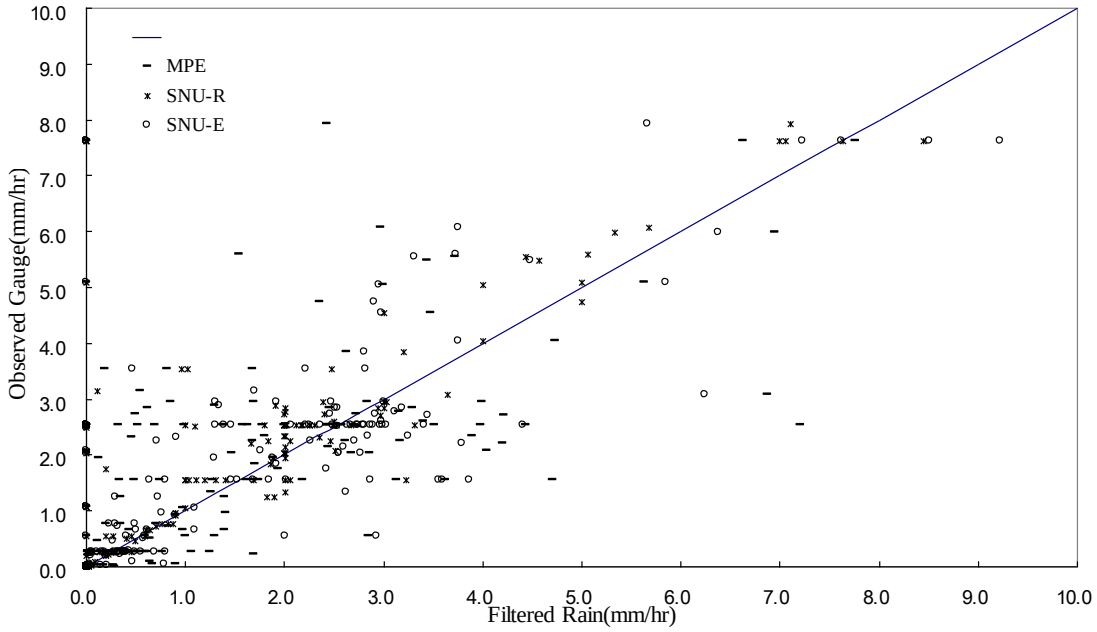

(b)

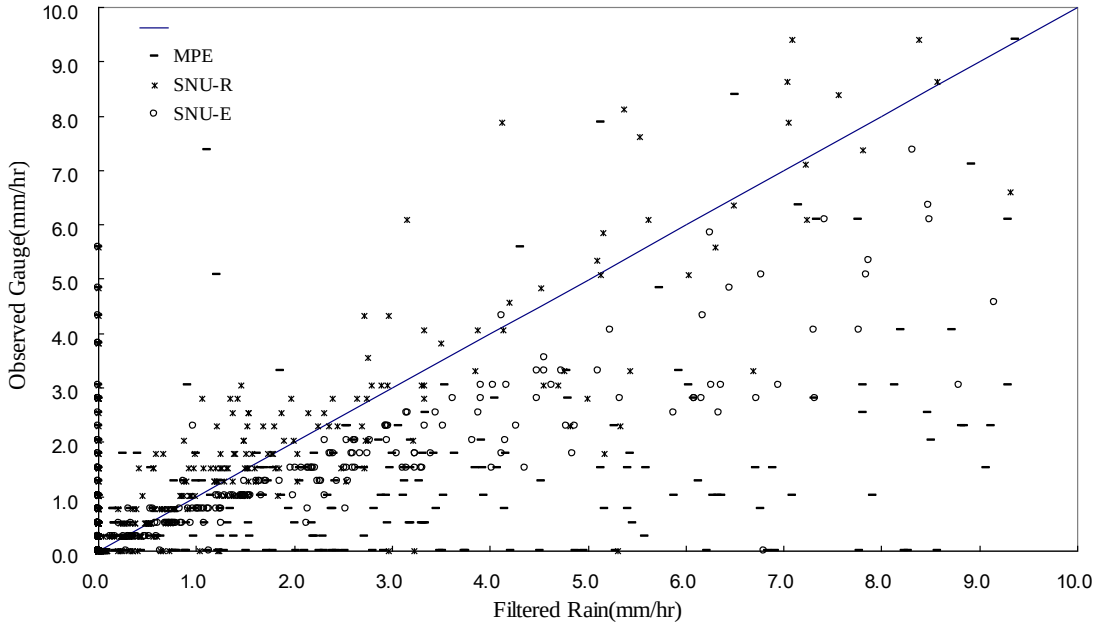

Figure 4.3 Scatter plot of NEXRAD bias corrected rainfall and cross–validated observed gauge rainfall for (a) the UWR and (b) the UCR basins.

Table 4.2 NEXRAD bias corrected rainfall statistics in the UWR basin.

Event	MPE scheme			SNU–R scheme			SNU–E scheme		
	RMSE (mm)	MAPE (%)	R^2	RMSE (mm)	MAPE (%)	R^2	RMSE (mm)	MAPE (%)	R^2
1	0.80	12.06	0.74	0.59	8.05	0.87	0.71	9.98	0.80
2	1.73	48.13	0.57	0.76	18.76	0.92	1.09	31.07	0.82
3	1.63	30.72	0.62	1.46	14.40	0.70	1.44	17.56	0.70
4	0.38	22.00	0.89	0.13	10.28	0.98	0.26	17.73	0.93
5	1.30	93.41	0.53	1.05	19.04	0.67	1.21	66.79	0.57
Ave.	1.17	41.26	0.67	0.80	14.11	0.83	0.94	28.63	0.76

Table 4.3 NEXRAD bias corrected rainfall statistics in the UCR basin.

Event	MPE scheme			SNU-R scheme			SNU-E scheme		
	RMSE (mm)	MAPE (%)	R^2	RMSE (mm)	MAPE (%)	R^2	RMSE (mm)	MAPE (%)	R^2
1	3.27	80.37	0.35	1.02	15.45	0.88	2.08	30.27	0.93
2	5.15	169.69	0.37	0.59	29.37	0.60	0.99	45.27	0.85
3	29.48	90.38	0.01	26.47	26.34	0.04	26.64	34.88	0.01
4	16.66	127.66	0.13	1.84	23.93	0.53	2.04	36.74	0.53
5	14.23	108.64	0.67	0.88	25.70	0.90	2.02	41.60	0.88
Ave.	13.76	115.35	0.30	6.16	24.16	0.58	6.75	37.75	0.64

(a)

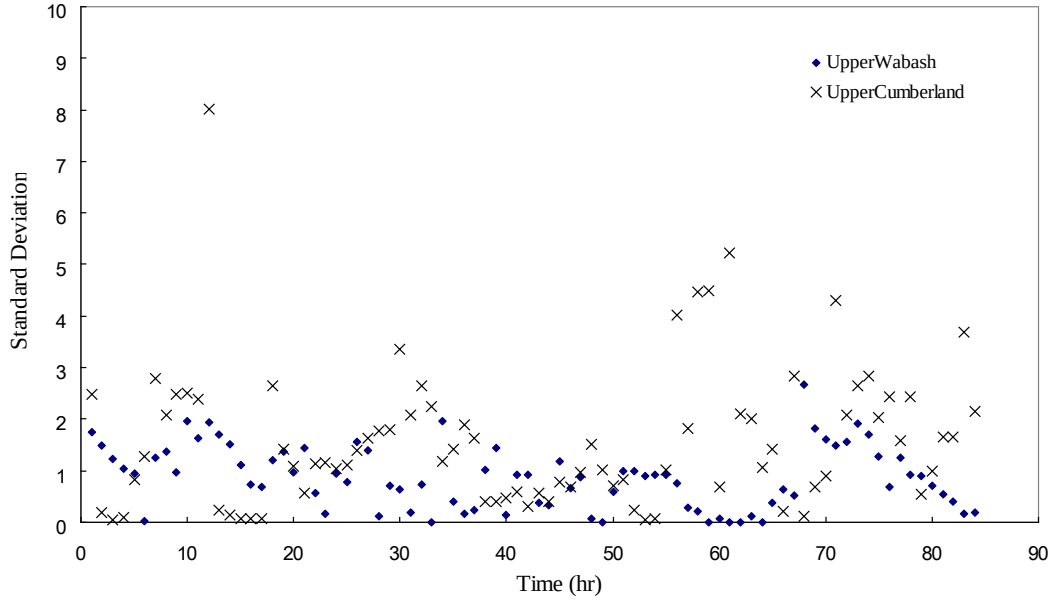

(b)

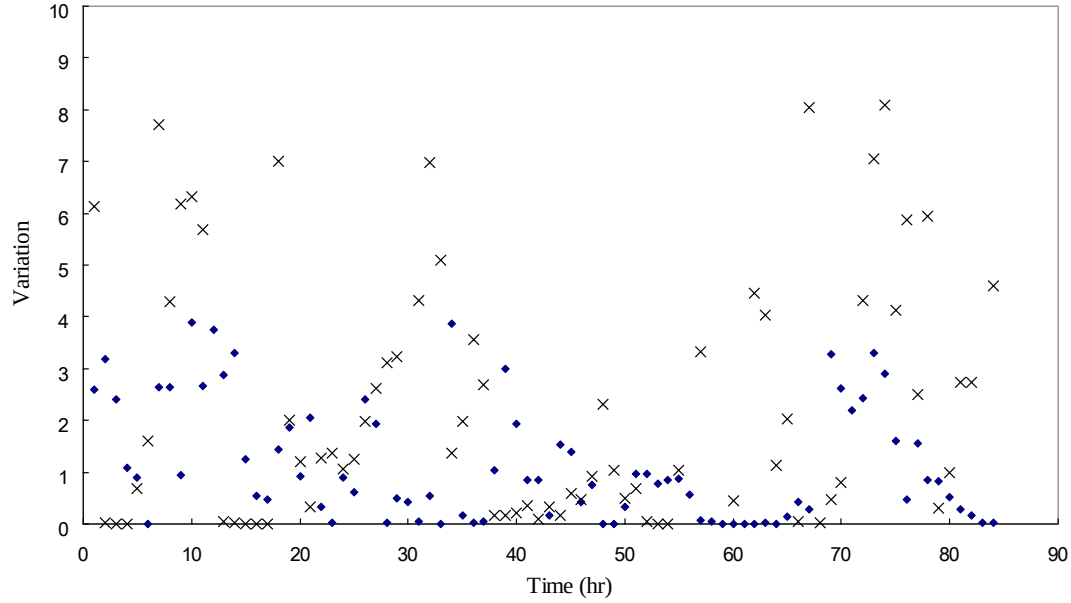

Figure 4.4 Time series of (a) Standard Deviation and (b) Variation.

4.4.2. Sensitivity of Hydrographs to NEXRAD Bias Correction Schemes

To study the sensitivity of model hydrograph to rainfall inputs obtained by using three different approaches for NEXRAD bias correction, the STORE DHM model is calibrated for each event for both watersheds. The model is manually calibrated by using the Nash–Sutcliffe coefficient (E_{NS}) for discharge and root mean square error (RMSE) for the total runoff volume. The RMSE are defined as

$$RMSE = \sqrt{\sum_{i=1}^{n} (Q_{sim}^{i} - Q_{obs}^{i})^2} \qquad \text{Eq. 4.1}$$

where Q_{sim} is the simulated hourly streamflow, and Q_{obs} is the observed hourly streamflow. Calibration factors used to adjust the model and the corresponding parameter values are presented in Tables 4.4 and 4.5. The results from calibration are presented in Figure 4.5 and Tables 4.6 and 4.7.

Table 4.4 Calibrated Manning's n values for each event in the UWR basin.

Event	Upper Wabash River Basin			
	Land Use Calibration			
	Agricultural	Forest	Developed	Water
1	0.023	0.013	0.011	0.006
2	0.020	0.019	0.015	0.005
3	0.019	0.014	0.011	0.006
4	0.025	0.020	0.018	0.006
5	0.018	0.015	0.013	0.005

Table 4.5 Calibrated Manning's n values for each event in the UCR basin.

Event	Upper Cumberland River Basin			
	Land Use Calibration			
	Agricultural	Forest	Developed	Water
1	0.051	0.035	0.033	0.016
2	0.081	0.055	0.043	0.026
3	0.061	0.036	0.023	0.020
4	0.062	0.043	0.037	0.012
5	0.054	0.037	0.035	0.015

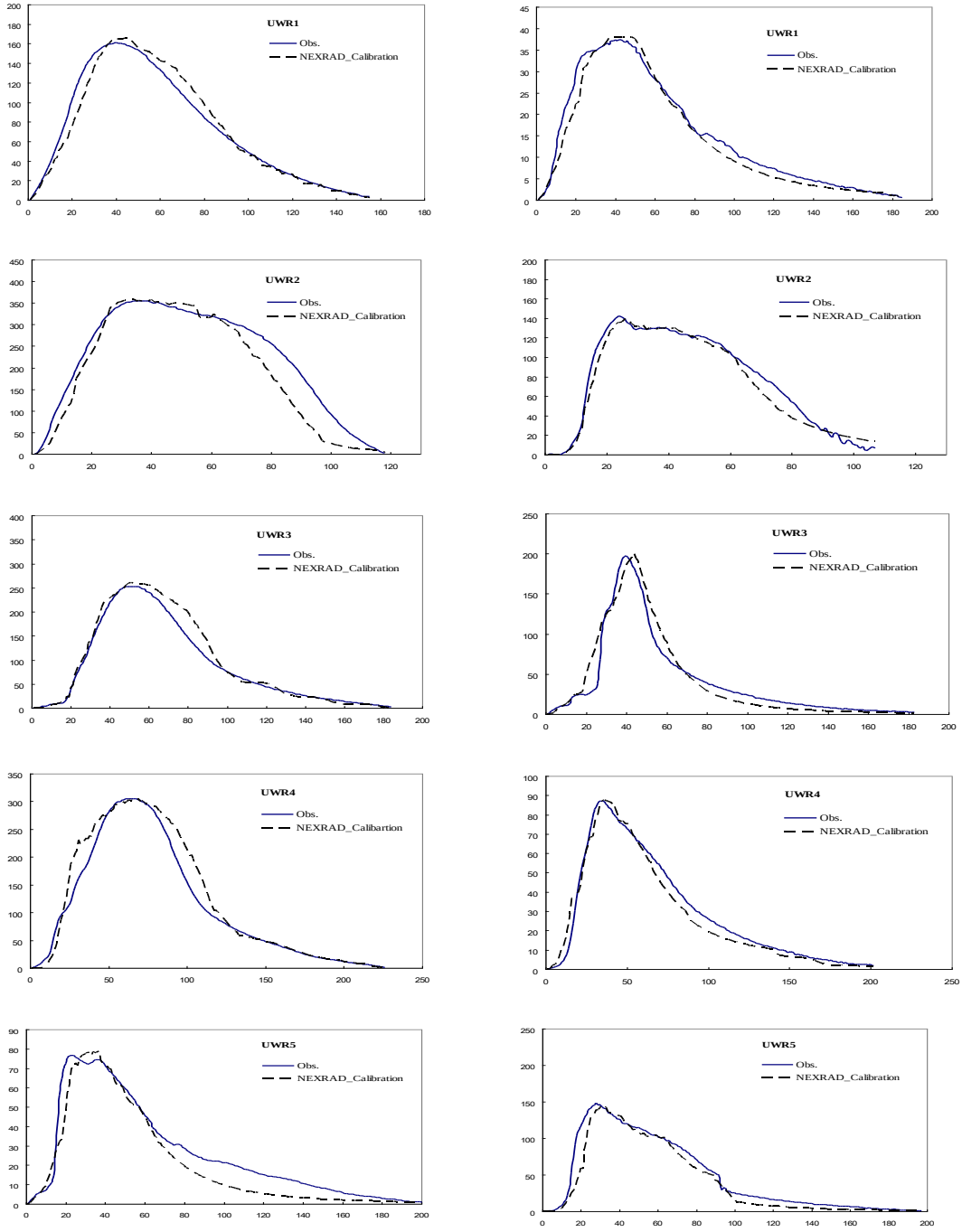

(a) UWR basin (b) UCR basin

Figure 4.5 Calibrated model results for every event using NEXRAD rainfall input (e.g. UWR1 represents event 1 for UWR basin). X–axis represents time in hours and Y–axis represents flow in cubic meters per second.

Table 4.6 Calibrated simulation statistics for each event in the UWR basin.

Event	Upper Wabash River Basin			
	Calibration with NEXRAD input			
	R^2	E_{NS}	RMSE(m^3/s)	MAPE(%)
1	0.98	0.97	2.21	14.58
2	0.97	0.97	9.13	19.56
3	0.94	0.93	13.49	37.59
4	0.98	0.97	4.70	27.45
5	0.95	0.93	12.83	33.89
Ave.	0.96	0.95	8.47	26.62

Table 4.7 Calibrated simulation statistics for each event in the UCR basin.

Event	Upper Cumberland River Basin			
	Calibration with NEXRAD input			
	R^2	E_{NS}	RMSE(m^3/s)	MAPE(%)
1	0.97	0.96	10.24	10.48
2	0.94	0.86	43.97	23.77
3	0.98	0.96	16.50	16.94
4	0.97	0.94	24.36	16.57
5	0.95	0.90	7.54	40.81
Ave.	0.96	0.93	20.52	21.72

After calibration, each event is simulated with the STRORE DHM using three variations of NEXRAD rainfall created by applying uniform and non–uniform spatial bias correction. The hydrographs from these simulations are presented in Figures 4.6–4.10, and results are summarized in Tables 4.8–4.13. For the UWR basin (Figs 4.6a–4.10a and Tables 4.8–4.10), the calibrated R^2 of 0.96 decreased to 0.92 for MPE, 0.95 for SNU–R, and 0.95 for SNU–E. The calibrated E_{NS} of 0.95 decreased to 0.82 for MPE, but remained unchanged for SNU–R and SNU–E. The calibrated RMSE of 8.47 m^3/s changed to 16.49 m^3/s for MPE, 9.86 m^3/s for SNU–R and 11.20 m^3/s for SNU–E. Similarly, the calibrated MAPE of 26.62% changed to 33.75% for MPE, 27.98% for SNU–R and 30.80% for SNU–E. Overall, SNU–R shown a 67% improvement in RMSE and 21% improvement in MAPE of the output hydrographs compared to hydrographs from MPE rainfall input. SNU–E shown a 47% improvement in RMSE and 10% in improvement in MAPE of the output hydrographs compared to hydrographs from MPE rainfall input.

For the UCR basin (Figs 4.6b–4.10b and Tables 4.11–4.13), the calibrated R^2 of 0.96 decreased to 0.80 for MPE, 0.94 for SNU–R, and 0.94 for SNU–E. The calibrated E_{NS} of 0.93 decreased to 0.65 for MPE, 0.88 for SNU–R, and 0.94 for SNU–E. The calibrated RMSE of 20.52 m^3/s changed to 47.36 m^3/s for MPE, 27.08 m^3/s for SNU–R and 24.73 m^3/s for SNU–E. Similarly, the calibrated MAPE of 21.72% changed to 54.75% for MPE, 26.99% for SNU–R and 26.56% for SNU–E. Overall, SNU–R shown a 75% improvement in RMSE and 103% improvement in MAPE of the output hydrographs compared to hydrographs from MPE rainfall input. SNU–E shown a 92% improvement in RMSE and 106% in improvement in MAPE of the output hydrographs compared to hydrographs from MPE rainfall input.

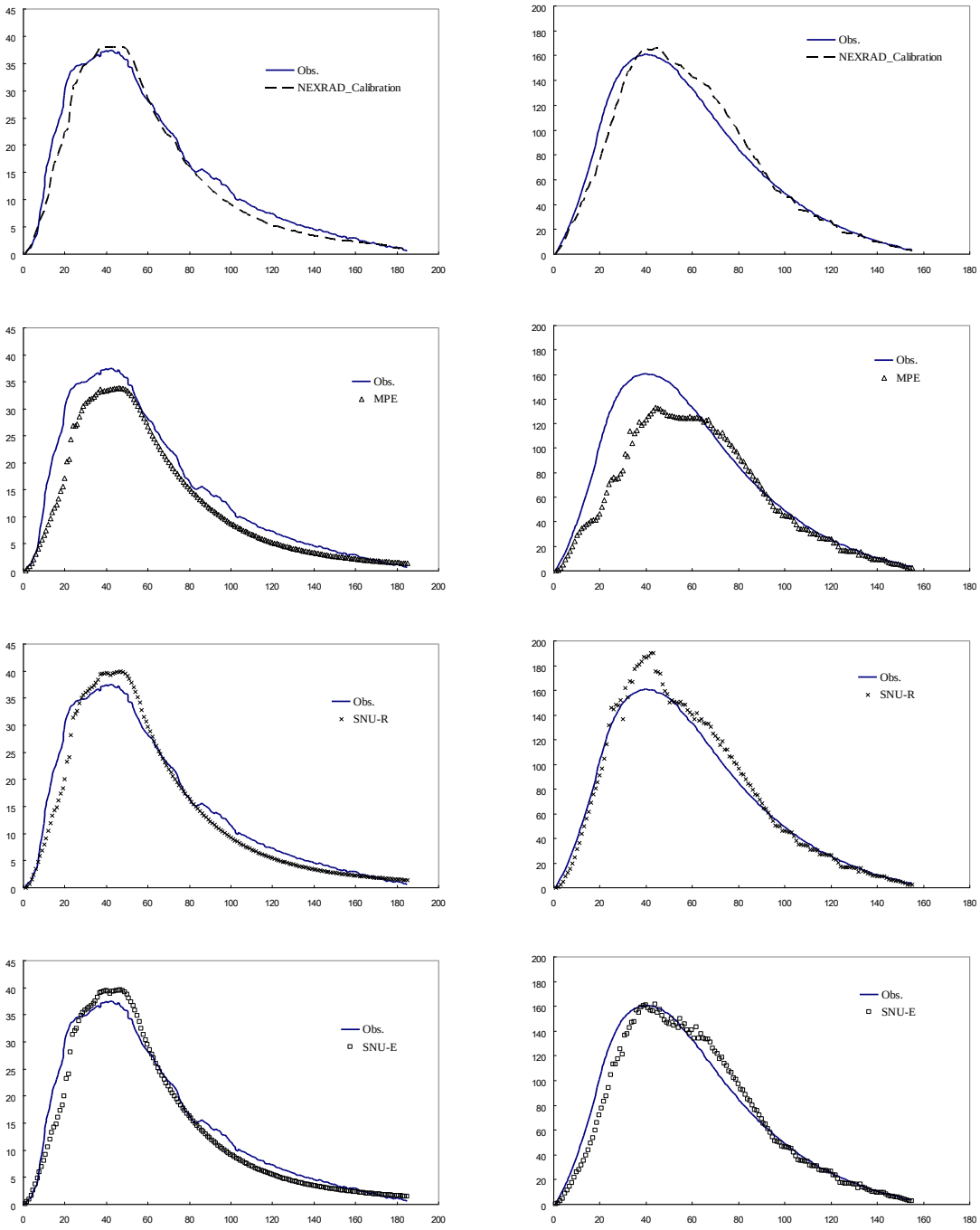

(a) UWR basin (b) UCR basin

Figure 4.6 Storm Event 1 model hydrographs for both (a) the UWR basin and (b) the UCR basin. X–axis represents time in hours and Y–axis represents flow in cubic meters per second.

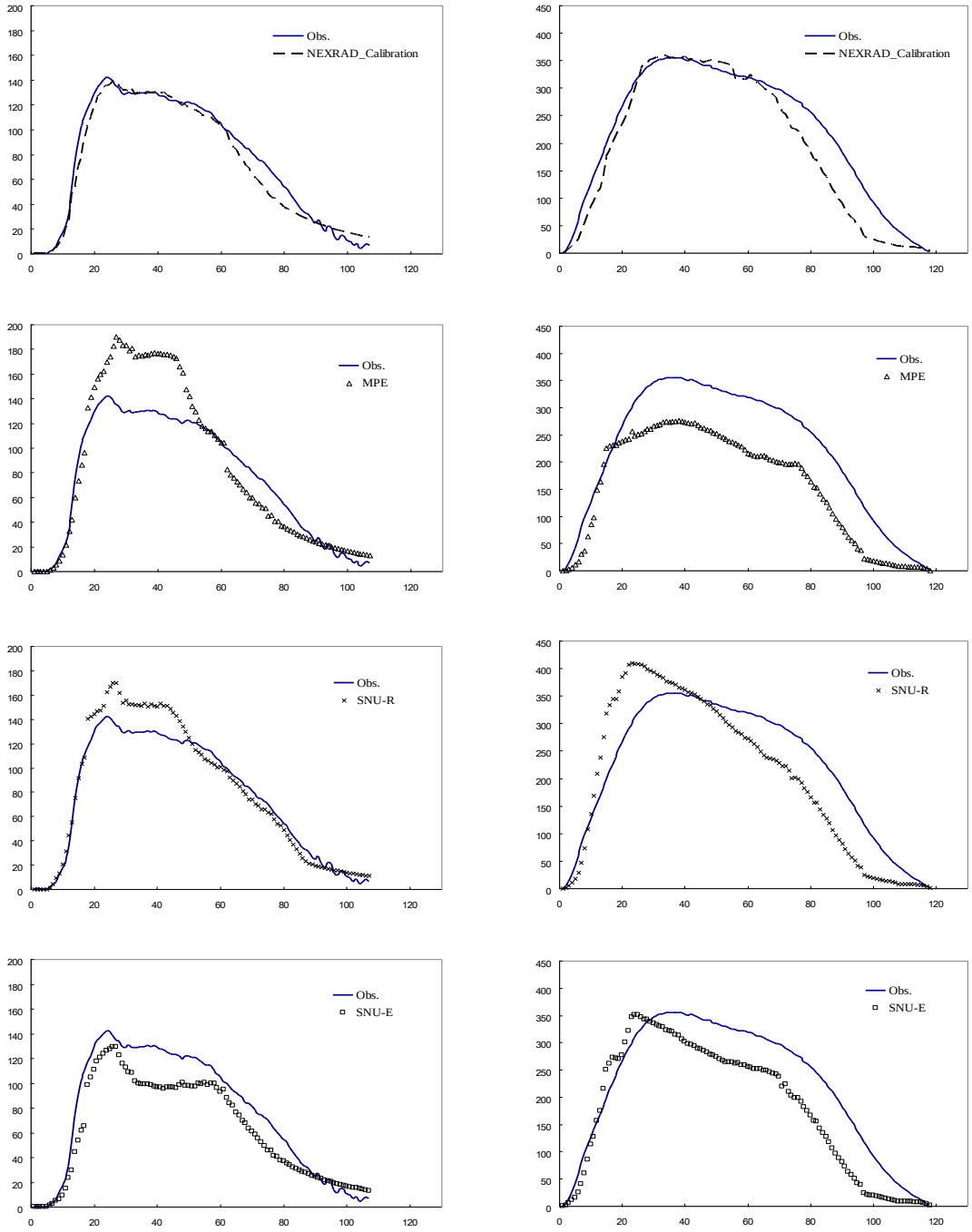

(a) UWR basin (b) UCR basin

Figure 4.7 Storm Event 2 model hydrographs for both (a) the UWR basin and (b) the UCR basin. X–axis represents time in hours and Y–axis represents flow in cubic meters per second.

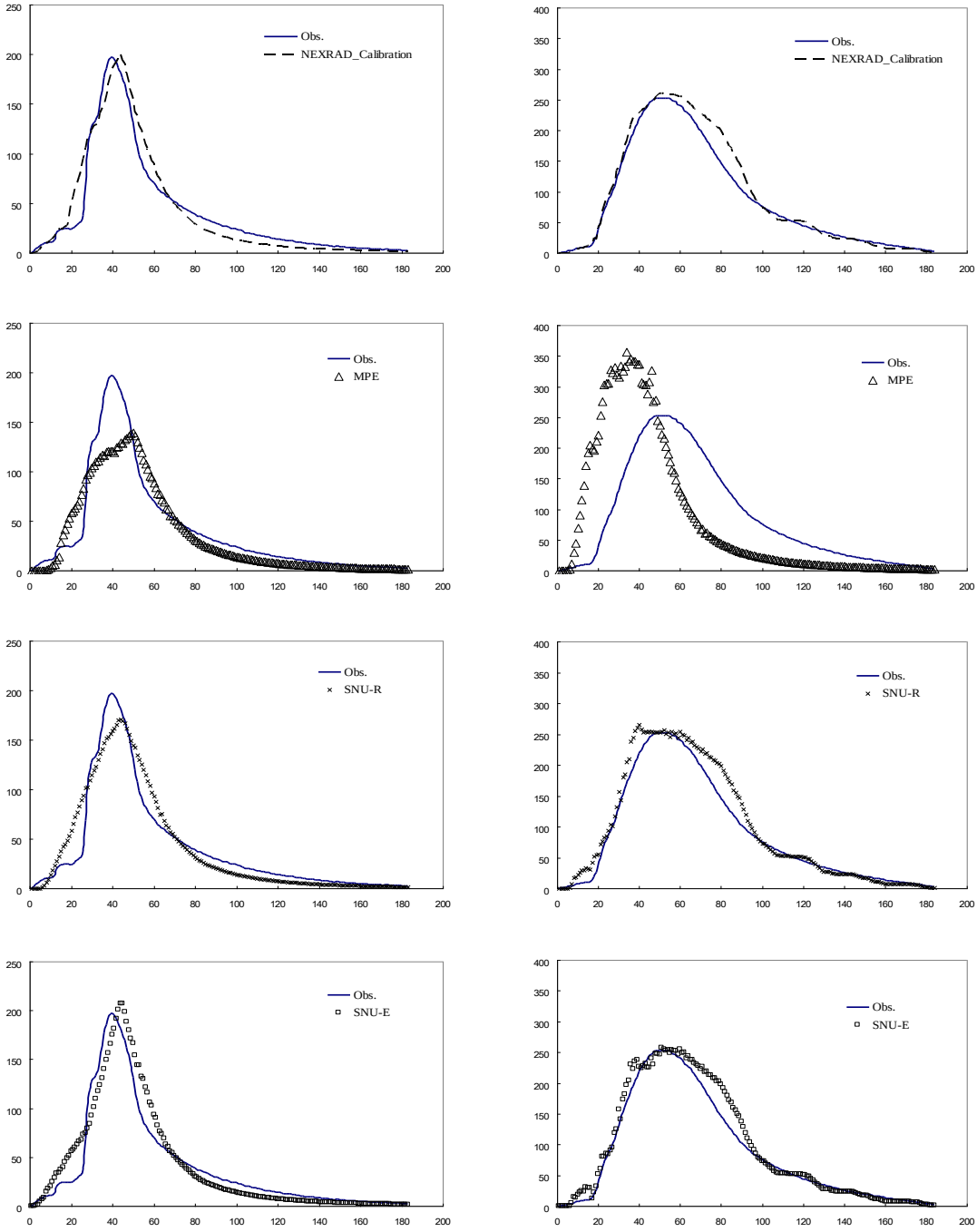

(a) UWR basin (b) UCR basin

Figure 4.8 Storm Event 3 model hydrographs for both (a) the UWR basin and (b) the UCR basin. X–axis represents time in hours and Y–axis represents flow in cubic meters per second.

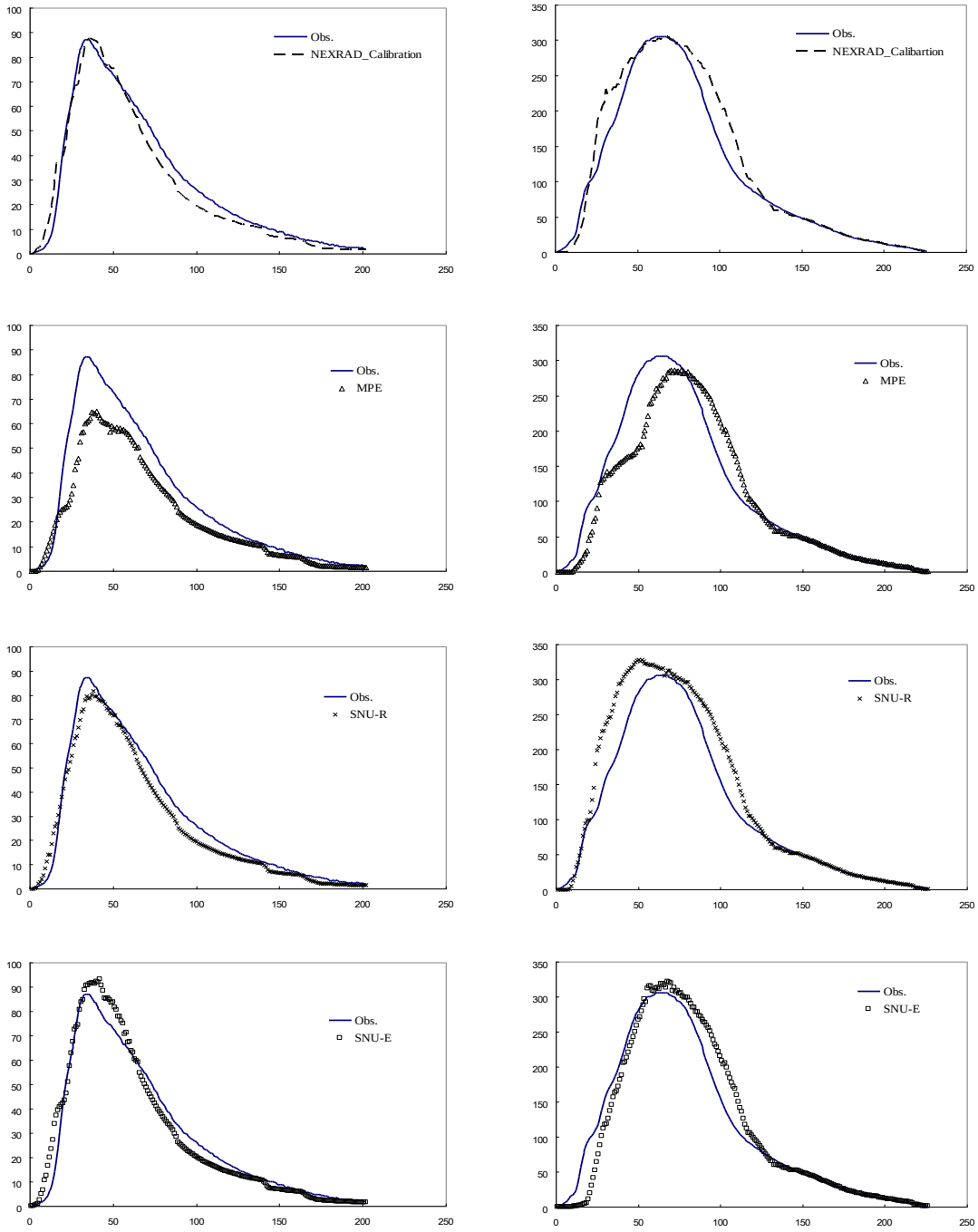

(a) UWR basin (b) UCR basin

Figure 4.9 Storm Event 4 model hydrographs for both (a) the UWR basin and (b) the UCR basin. X–axis represents time in hours and Y–axis represents flow in cubic meters per second.

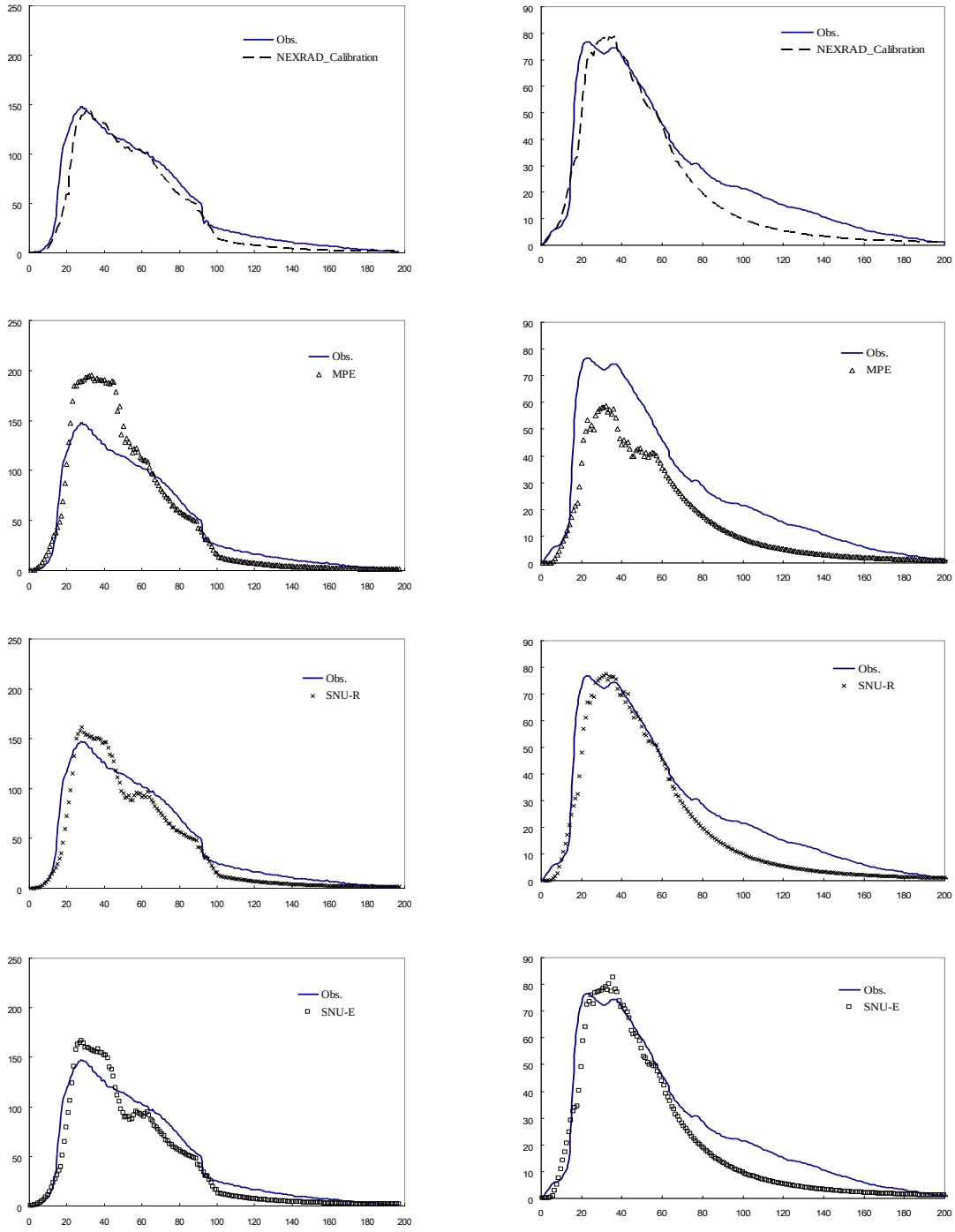

(a) UWR basin (b) UCR basin

Figure 4.10 Storm Event 5 model hydrographs for both (a) the UWR basin and (b) the UCR basin. X–axis represents time in hours and Y–axis represents flow in cubic meters per second.

Table 4.8 Details of simulation results with MPE NEXRAD bias corrected rainfall input for the UWR basin.

Event	Simulation with MPE scheme			
	R^2	E_{NS}	RMSE(m^3/s)	MAPE(%)
1	0.96	0.92	3.51	21.48
2	0.90	0.72	25.83	30.30
3	0.86	0.84	20.43	41.58
4	0.96	0.85	10.63	29.46
5	0.94	0.79	22.08	45.95
Ave.	0.92	0.82	16.49	33.75

Table 4.9 Details of simulation results with SNU–R NEXRAD bias corrected rainfall input for the UWR basin.

Event	Simulation with SNU–R scheme			
	R^2	E_{NS}	RMSE(m^3/s)	MAPE(%)
1	0.97	0.96	2.56	18.18
2	0.97	0.93	13.13	19.59
3	0.91	0.91	15.54	40.42
4	0.98	0.97	4.94	27.48
5	0.95	0.93	13.12	34.22
Ave.	0.95	0.94	9.86	27.98

Table 4.10 Details of simulation results with SNU–E NEXRAD bias corrected rainfall input for the UWR basin.

Event	Simulation with SNU–E scheme			
	R^2	E_{NS}	RMSE(m^3/s)	MAPE(%)
1	0.97	0.96	2.53	18.19
2	0.96	0.86	18.38	28.24
3	0.91	0.90	16.24	41.26
4	0.97	0.96	5.35	28.63
5	0.94	0.92	13.49	37.66
Ave.	0.95	0.92	11.20	30.80

Table 4.11 Details of simulation results with MPE NEXRAD bias corrected rainfall input for the UCR basin.

Event	Simulation with MPE scheme			
	R^2	E_{NS}	RMSE(m^3/s)	MAPE(%)
1	0.88	0.81	23.24	17.40
2	0.92	0.60	74.64	37.95
3	0.36	0.19	92.02	149.85
4	0.89	0.89	34.51	19.66
5	0.95	0.73	12.40	48.90
Ave.	0.80	0.65	47.36	54.75

Table 4.12 Details of simulation results with SNU–R NEXRAD bias corrected rainfall input for the UCR basin.

Event	Simulation with SNU–R scheme			
	R^2	E_{NS}	RMSE(m^3/s)	MAPE(%)
1	0.99	0.97	9.42	10.81
2	0.82	0.70	65.16	32.74
3	0.97	0.95	19.48	30.89
4	0.96	0.89	33.74	18.51
5	0.95	0.90	7.59	42.00
Ave.	0.94	0.88	27.08	26.99

Table 4.13 Details of simulation results with SNU–E NEXRAD bias corrected rainfall input for the UCR basin.

Event	Simulation with SNU–E scheme			
	R^2	E_{NS}	RMSE(m^3/s)	MAPE(%)
1	0.96	0.96	11.42	12.69
2	0.89	0.75	59.06	31.22
3	0.97	0.95	18.25	26.69
4	0.94	0.93	27.27	18.76
5	0.94	0.90	7.64	43.42
Ave.	0.94	0.90	24.73	26.56

(a)

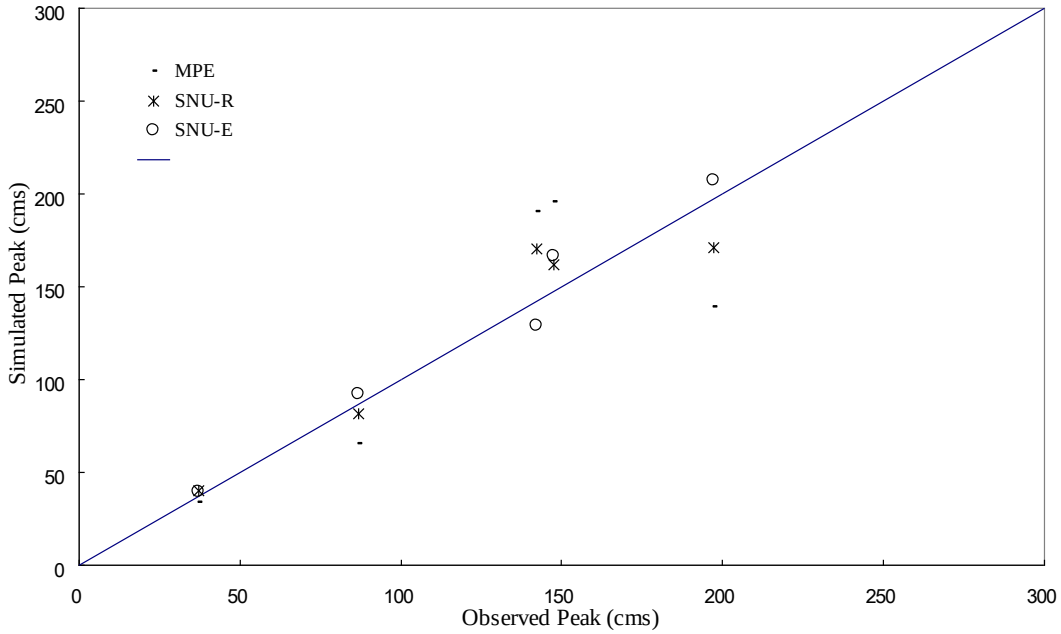

(b)

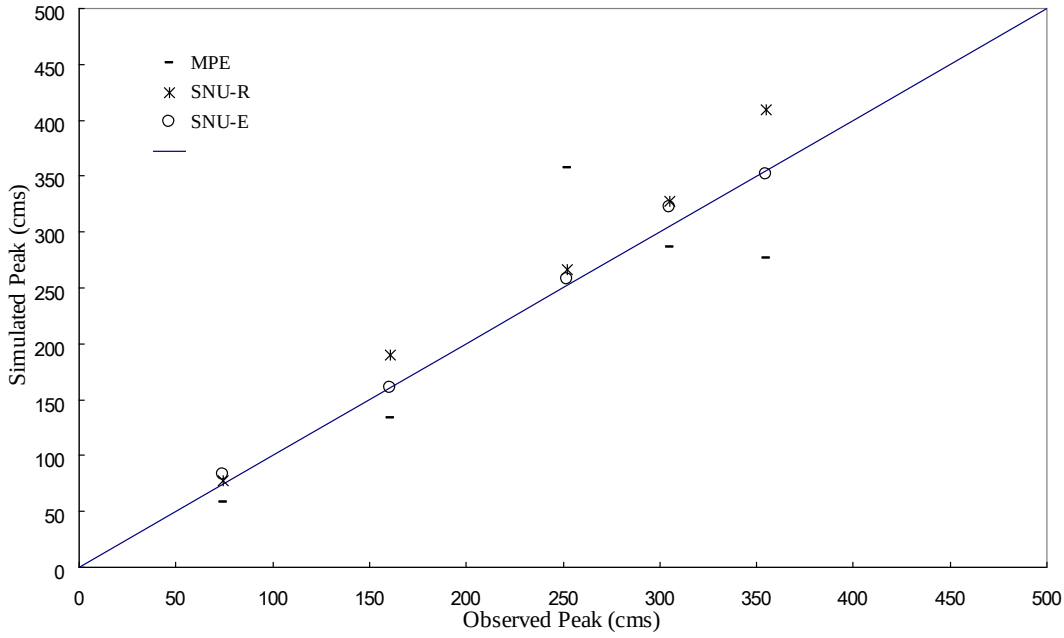

Figure 4.11 Storm events peak discharge (m^3/s) scatter plots for (a) the UWR and (b) the UCR basins.

The rainfall input derived by applying spatially uniform bias correction to NEXRAD data decreased calibrated model prediction accuracy as evident from R^2, E_{NS}, RMSE and MAPE values in comparison to input derived by applying spatially non–uniform bias correction scheme. The improvement in model results from spatially non–uniform bias corrected input are better in UCR basin compared to UWR basin because the NEXRAD values are more variable in time over UCR basin compared to UWR basin as shown in Fig. 4.4.

Even though the NEXRAD input is adjusted by using gauged rainfall, some under–prediction or over–prediction of runoff volume and peak flow are found in both study areas as shown in Figs. 4.6–4.10. Simulations with SNU–E inputs performed the best with regard to the estimation of peak flow as shown in scatter Fig. 4.11. Similarly, the input from both methods using spatially non–uniform bias correction produced overall better output compared to input from spatially uniform bias correction method in terms of total runoff volume.

4.5. Summary and Conclusions

Three NEXRAD bias corrections are presented in this study. To evaluate the sensitivity and accuracy of NEXRAD bias corrected rainfall, the Upper Wabash River and the Upper Cumberland River basins is selected because of different spatial characteristics. Suggested NEXRAD bias correction schemes are applied to the study basins to evaluate effects of each NEXRAD bias correction scheme on the variation of NEXRAD distribution. Simultaneous comparisons of three NEXRAD bias corrected rainfall are made to cross validate with observed gauge rainfall at down, middle and up location of two study basins (Fig. 4.1). Improvement in the accuracy of rainfall is achieved through adjustment of spatially non–uniform NEXRAD bias correction at the two watersheds in comparison with spatially uniform NEXRAD bias correction. Overall, spatially non–uniform NEXRAD bias correction performance in comparison to MPE

scheme improves from 1.17 to 0.87 mm RMSE in the Upper Wabash River basin, and from 13.76 to 6.45 mm RMSE in the Upper Cumberland River basin. Spatially non–uniform NEXRAD bias correction reduces accuracy error in the Upper Wabash River basin from 41.26% MAPE to 21.37% MAPE, whereas in the Upper Cumberland River Basin, a large reduction is obtained, 115.35% MAPE to 30.96% MAPE. Use of spatially non–uniform NEXRAD bias correction in large variability of NEXRAD distribution over the entire watershed such as the Upper Cumberland River basin is more effective than small variability of NEXRAD distribution over the entire watershed such as the Upper Wabash river Basin.

When a spatially uniform bias corrected rainfall input is used in the STORE DHM, prediction accuracy is degraded. Spatially uniform bias corrected rainfall input produces inconsistent results with both over prediction and under prediction and no clear trend. To evaluate sensitivity of rainfall accuracy on hydrologic model simulation, calibrated parameters in each event are obtained from simulation with original NEXRAD. These calibrated parameters then are applied to the STORE DHM with three different schemes of NEXRAD bias corrected rainfall. The accuracy of model prediction with different NEXRAD bias corrected rainfall is estimated in terms of the R^2, E_{NS}, RMSE and MAPE based on observed data combination. Spatially non–uniform NEXRAD bias corrected rainfall improves prediction accuracy in both the Upper Wabash River and the Upper Cumberland River basins. However, a reduction in accuracy of model prediction is shown in both study areas, when model is used with spatially uniform NEXRAD bias corrected rainfall. An interpolation scheme that accounts for the spatially non–uniform NEXRAD bias is applied for reducing spatio–temporal variation of NEXRAD bias. The spatially non–uniform NEXRAD bias correction proposed in this study uses two different schemes. Even though these schemes have different procedures before trying the Kalman filtering, the STORE DHM model simulations with these two NEXRAD bias corrected rainfall produced nearly equivalent prediction accuracy error statistics and peak flow error for the events tested that are consistent with both the Upper Wabash River and the Upper Cumberland River basins.

Testing sensitivity to variation of NEXRAD values distribution reveals that the improvement of prediction accuracy with spatially non–uniform NEXRAD bias corrected rainfall is greater in larger NEXRAD variation area, whereas, prediction accuracy in smaller NEXRAD variation area is less improved in comparison to simulation with MPE scheme rainfall. The large NEXRAD variation at a certain time step implies that each NEXRAD pixel bias is not uniform, thus NEXRAD bias correction with spatially non–uniform scheme is much more effective than uniform NEXRAD bias correction scheme. To evaluate this investigation, this study selects two different characteristics of study areas: the Upper Wabash River basin has flat terrain with less rainfall variability, and the Upper Cumberland River basin with relatively mountainous terrain and more variable rainfall. The results in comparison to simulation with spatially uniform NEXRAD bias corrected rainfall show that prediction accuracy with spatially non–uniform NEXRAD bias corrected rainfall in the Upper Cumberland River basin shows more improvement compared to the Upper Wabash River basin. Consequently, spatially non–uniform NEXRAD bias correction is an efficient scheme for high NEXRAD variability areas.

CHAPTER 5. RESEARCH SYNTHESIS AND FURTURE WORK

5.1. Object–oriented hydrologic model

This research is focused on developing a prototype GIS based tightly coupled object–oriented framework called GHISMO. The GHISMO has an object–oriented approach using object–oriented design techniques and object–oriented language, Visual Basic, to the description and simulation of a watershed based hydrologic process. The GHISMO allows flexibility and extensibility to investigate future hydrologic issues without changing its main framework because it uses characteristics of inheritance and aggregation through an object–oriented hydrologic approach. For example, if object–oriented based hydrologic models try large scale programming components (infiltration, Green–Ampt and SCS curve number) at the same time, object–oriented programming can be easy to manage because each object has a component which has an individual method and property based on the object class.

Expanding of the GHISMO framework will be essential for robustness of the hydrologic model. For example, linkage between GHISMO and water quality model (e.g., SWAT) can predict effect of storm event on water quality assessment. Similarly, linkage between the GCMs (General Circulation Models), which are the most advanced tools for estimating future climate change, and GHISMO will provide a foundation to assess the impact of climate change on rainfall–runoff prediction. The conceptualization and characterization of this coupling strategy can be extended to a hydrologic management and decision supporting tool such as a real–time flood warning system. If the prototype of the object–oriented hydrologic framework, the GHISMO, is successfully used to develop a coupled open source and platform for seamless hydrologic components, it may lead to

change a hydrologic modeling paradigm to object-oriented approach through its flexible modeling schemes.

5.2. Parameter Estimation for STORE DHM

Surface roughness has a significant effect on runoff peak flow and time to peak in rainfall–runoff simulation. Although STORE DHM simulations (the first part of the broader GHISMO framework) show promising results in comparison with observed hydrographs, the issue for estimation of surface roughness in different land surface types is still open to dispute because model calibration only rely on surface roughness for runoff peak flow and time to peak. For example, surface roughness parameter values at Fish Creek simulations are out of land use range values (which are provided by Brater and King (1976)). Also, even though calibrated surface roughness values for each event are obtained from the same study area (UWR or UCR basin), each calibrated surface roughness value in the same study shows difference in each land use type.

5.3. Critical Cell Travel Time Criteria

This research suggests CCT to overcome the DEM issue for STORE DHM simulations. To avoid different simulation results depending on DEM size, this research uses minimum simulation time step at each event in the particular region. Even though CCT is theoretically ideal approach for STORE DHM simulation, it still needs to be refined for physical approach to other hydrologic components and its boundary condition depending on event types (e.g., small, medium and heavy storm events) and study areas.

5.4. Number of Rain gauge for correcting radar bias

Rainfall is a critical factor in hydrologic simulation. However, rainfall varies substantially in space and time and therefore it is often poorly represented in hydrologic models. Even though radar rainfall provides a better spatial representation of rainfall variability, it still suffers from uncertainties and biases. To overcome this limitation, this research suggests three radar rainfall bias correction schemes (e.g., MPE, SNU–R and SNU–E). The research results suggest that spatially non–uniform radar bias correction schemes in large radar variation area are a higher improvement of radar bias correction over small radar variation area, both in regards to analysis of correcting radar bias and prediction accuracy of the STORE DHM with different radar bias corrected rainfall. However, the fundamental issue of minimum number of rain gauge information for correcting radar bias remains.

LIST OF REFERENCES

Adisoma, G.S., and Hester, M.G., 1996. Grade estimation and its precision in mineral resources: the Jackknife approach. Mining Engineering 48(2), 84–88.

Abbott, M.B., Bathurst, J.C., Cunge, P.E., Rasmussen, J., 1986. An introduction to the European hydrological system– System hydrologique europeen, "SHE", 1: Distributed modeling system. Journal of Hydrology 87, 45–59.

Ajward, M.H., 1996. A spatially distributed unit hydrograph model using a geographic information system. Ph.D. Dissertation, Civil Engineering Department, University of Calgary, Calgary.

Anagnostou, E.N., Krajeswski, K.F., Smith, J., 1999. Uncertainty quantification of mean real radar–rainfall estimates. Journal of Atmospheric and Ocean Technology 16, 206–215

Band, L.E., Tague, C.L., Brun, S.E., Tenenbaum, D.E., Frernandez, R.A., 2000. Modeling watersheds as spatial object hierarchies: structure and dynamics. Transaction in GIS 4(3), 181–196.

Beven, K., Moore, I., 1993. Terrain analysis and distributed modeling in hydrology. John Wiley and Sons: New York.

Beven, K., 2002. Towards an alternative blueprint for a physically based digitally simulated hydrologic response modeling system. Hydrologic Process 16, 189–206.

Bian, L., Object–oriented representation of environmental phenomena: Is everything best represented as an object. Annals of the Association of American Geographers 97(2), 267–281.

Borga, M., Anagnostou, E.N., Enrico, F., 2000. On the use of real time radar rainfall estimates for flood prediction in mountainous basins. Journal of Geophysical Research 105(D2), 2269–2280.

Boyer, J.F., Berkhoff, C., Servat, E., 1996. Object–oriented programming for a simulation of the rainfall–discharge relationship. In: proceedings of Hydroinformatics 96. Balkema, A.A. Zurich, Switzerland, pp. 299–305.

Brater, E.F., King, H.W., 1976. Handbook of Hydraulics for the Solution of Hydraulic Engineering Problems, McGraw–Hill Book Company, New York, USA.

Bronstert, A., Plate, E.J., 1997. Modeling of runoff generation and soil moisture dynamics for hillslopes and microcatchment. Journal of Hydrology 198, 177–195.

Calver, A., Wood, W.L., 1995, The Institute of Hydrology Distributed Model, In: Shigh, V.P. (Eds.), Computer Models of Watershed Hydrology, Water resources Publication, Colorado, pp. 595–626.

Carpenter, T.M., Georgakakos, K.P., Sperfslage, J.A., 2001. On the parametric and NEXRAD–radar sensitivities of a distributed hydrologic model suitable for operational use. Journal of Hydrology 254, 169–193.

Chen, H., Beschta, R., 1999. Dynamic hydrologic simulation of the Bear Brook Wathershed in Maine (BBWM). Environmental Monitoring and Assessment 55, 53–96.

Chow, V.T., Maidment, D.R., Mays, L.W., 1988. Applied Hydrology, McGraw Hill Publishing, New York, 572 pp.

Ciach, G..j., Krajewski, W.F., 1999. Radar rain gauge comparisons under observational uncertaintities. Journal of Applied Meteorology 38, 1519–1525.

Desmet, P., Govers G., 1998. Comment on ‘Modeling topographic potential for erosion and deposition using GIS’. International Journal of Geographical Information Science 10:311–331.

Dinku, T., Ananostou, E.N., Borga, M., 2002. Improving radar–based estimation of rainfall over complex terrain. Journal of Applied Meteorology 41, 1163–1178.

Du, J., Xie, H., Xu, Y., Xu, C., 2009. Development and testing of a new storm runoff routing approach based on time variant spatially distributed travel time method. Journal of Hydrology 369, 44–54.

Fairfield, J., Leymarie, P., 1991. Drainage networks from grid digital elevation models. Water Resources Research 27(5), 709–717.

Famiglietti, J.S., Wood, E.F., 1994. Multiscale modeling of spatially variable water and energy balance processes. Water Resources Research 30(11), 3061–3078.

Faures, J.M., Goodrich, D.C., Woolhiser, D.A., Sorooshian, S., 1995. Impact of small–scale rainfall variability on runoff modeling. Journal of hydrology 173, 309–326.

FitzHugh, T.W., Mackay, D.S., 2000. Impacts of input parameter spatial aggregation on an agricultural nonpoint source pollution model, Journal of Hydrology 236, 35–53.

Fulton, R.A., Breidenbach, J.P., Seo, D., Miller, D.A., O'Bannon, T., 1998. The WSR–88D rainfall algorithm. Weather and Forecasting 13, 377–395.

Garrote, L., Becchi, I., 1997. Object–oriented software for distributed rainfall–runoff models. Journal of Computing in Civil Engineering 11, 190–194.

Goldberg, A. and Rubin, K., 1995. Succeeding with objects. Decision Framework for Project Management. Addison Wesley Publishing Company, 1995. ISBN 0–201–62878–3.

Goodchild, M., Parks, B., Steyaert, L., 1993. Environmental Modeling with GIS. Oxford University Press: Oxford.

Gupta, R.S., 1995. Hydrology and Hydraulic Systems, Waveland Press, 739 pp.

He, C., Croley II, Thomas, E., 2007. Application of a distributed large basin runoff model in the Great Lakes basin. Control Engineering Practice 15(8), 1001–1011.

HEC–GeoRAS user's manual available at www.hec.usace.army.mil/software/hec–ras/hecgeoras.html.

HEC–RAS user's manual available at www.hec.usace.army.mil/software/hec–ras/

Johnson, L.E., 1989. MAPHYD–A digital map–based hydrologic modeling system. Photogrammetric Engineering and Remote Sensing, 55(6), 911–917.

Kang, K., Merwade, V., 2009. Effects of rain gage density on correcting radar precipitation and its influence on hydrologic model simulation, EOS Transactions AGU, 90(52), Fall meeting, San Francisco, CA, December 2009.

Kiker, G.A., Clark, D.J., Martinez, C.J., Schulz, R.E., 2006. A java based, object–oriented modeling system for southern African hydrology. Transactions of ASABE 49 (5), 1419–1433.

Kilgore, R.T., Krolak, J.S., Walsh, M., 1994. Integration of water resource models and GIS for water resource management. Water Policy and Management: Solving the Problems; Process, Conference, ASCE, New York, 37–40.

Koren, V., Smith, M., Duan, Q., 2003. Use of a priori parameter estimates in the derivation of spatially consistent parameter sets of rainfall–runoff models. In: Daun, Q., Sorooshian, S., Gupta, H., Rosseau, A., Turotte, R. (Eds.), Calibration of Watershed Models, AGU Water Science and Applications Series.

Kralisch, S., Krause, P., David, O., 2005. Using the object modeling system for hydrological model development and application. Advances in Geosciences 4, 75–81.

Lahlou, M., Shoemaker, L., Choudry, S., Elmer, R., Hu, A., Manguerra, H., Parker, A., 1998. Better assessment science integration point and nonpoint sources: BASIN 2.0 User's Manual. EPA–823–B–98–006, U.S. Environmental Protection Agency, Office of Water, Washington, DC, USA.

Lal, A.M.W., Van Zee, R., Belnap, M., 2005. Case study: model to simulate regional flow in South Florida. Journal of Hydraulic Engineering 131(4), 247–258.

Legates, D.R., 2000. Real–time calibration of radar precipitation estimates. Professional Geographer 52(2), 235–246.

Leipnick, M.R., Kemp, K.K., Loaiciga, H.A., 1993. Implementation of GIS for water resources planning and management. Journal of Water Resource Planning and Management 119(2), 184–205.

Li, M., Shao, Q., 2010. An improved statistical approach to merge satellite rainfall estimates and raingauge data. Journal of Hydrology, In press.

Liu, Y.B., Gebremeskel, S., Smedt, F., Hoffmann, L., Pfister, L., 2003. A diffusive transport approach for flow routing in GIS–based flood modeling. Journal of Hydrology 283(1–4), 91–106.

Looper, J., Vieux, B., Moreno, M., 2009. Assessing the impacts of precipitation bias on distributed hydrologic model calibration and prediction accuracy. Journal of Hydrology, In press.

Loucks, D.P., Kindler, J. and Fedra, K., 1985. Interactive water resources modeling and model use: An overview. Water Resources Research, 21(2), 95–102.

Luzio, Di, M., Srinivasan, R., Arnodl, J. G., Neitsch, S. L., 2002. Arcview Interface for SWAT2000. User's Guide. U.S. Department of Agriculture, Agriculture Research Service. Temple, Texas.

Maidment, D.R., 1993. GIS and hydrologic modeling. In: Goodchild, M., Parks, B., Steyaert, L. (Eds.), Environmental Modeling With GIS. Oxford University Press, New York, USA.

Maidment, D.R., Olivera, J.F., Calver, A., Eatherall, A., Fraczek, W., 1996. A unit hydrograph derived from a spatially distributed velocity field. Hydrologic Processes 10, 831–844.

Maidment, D.R., 2002. ArcHydro GIS for Water Resources, ESRI Press, California, 203 pp.

Madsen, H., 2003. Parameter estimation in distributed hydrological catchment modeling using automatic calibration with multiple objectives. Advances in Water resources 26(2), 205–216.

McKim, H.L., Cassell, E.A., Lapotin, P.J., 1993. Water resource modelling using remote sensing and object–oriented simulation. Hydrological Processes 7, 153–165.

Melesse, A.M., 2002. Spatially distributed storm runoff modeling using remote sensing and geographic information system. Ph. D. Dissertation, University of Florida.

Melesse, A.M., Graham, W.D., 2004. Storm runoff prediction based on a spatially distributed travel time method utilizing remote sensing and GIS. Journal of the American Water Resources Association 40(4), 863–879.

Molnar, D.K., Julien, P.Y., 2000. Grid–size effects on surface runoff modeling. Journal of Hydrol. Eng. ASCE 5 (1), 8–16.

Montgomery, D., Dietrich, W., 1994. A physically based model for the topographic control on shallow landsliding. Water Resources Research 30, 1153–1171.

Moore, I., Grayson, R., Ladson, A., 1991. Digital terrain modeling: a review of hydrological, geomorphological and biological applications. Hydrologic Processes 5, 3–30.

Moreda, F., Koren, V., Zhang, Z., Reed, S., Smith M., 2006. Parameterization of distributed hydrological models: learning from the experiences of lumped modeling. Journal of Hydrology 320(1–2), 218–237.

Muzic, I., 1995. GIS derived distributed unit hydrograph, a new tool for flood modeling. In: Topping, B. (Ed.), Developments in Computer Aided Design and Modeling for Civil Engineering. Civil–Component Press, Edinburgh, UK, pp. 243–247.

Muzic, I. 1996. Lumped modeling and GIS in flood prediction. Geographical Information Systems in Hydorlogy, Kluwer Academic Publishers.

Nash, J.E., and J.V. Sutcliffe. 1970. River flow forecasting through conceptual models: Part 1. A discussion of principles. Journal of Hydrology 10(3), 282–290.

Nelson, E. J., 1997. WMS v5.0 Reference Manual, Environmental Modeling Research Laboratory, Brigham Young University, Provo, Utah.

Nelson, E. J., Jones, N. L., and Jorgeson, J. D., 1995. A comprehensive environment for watershed modling and hydrologic analysis. Process, Conference, ASCE, New York, 897–901.

Nuss, W.A. and Titley, D.W., 1990. Use of multiquadric interpolation for meteorological objective analysis. Monthly Weather Review 122, 1611–1631.

O'Callaghan, J.F., Mark, D.M., 1984. The extraction of drainage networks from digital elevation data. Computer Vision, Graphics and Image Processing 28, 324–344.

Ogden, F.L., garbrecht, J., DeBarry, P.A., Johnson, L.E., 2001. GIS and distributed watershed models, II: Modules, interfaces and models. Journal of Hydrologic Engineering 6(6), 515–523.

Olivera, F., Maidment, D., 1999. Geographic Information System (GIS)–based spatially distributed model for runoff routing. Water Resources Research 35(4), 1155–1164.

O'Loughlin, E., 1986. Prediction of surface saturation zones in natural catchments by topographic analysis. Water Resources Research 22: 794–804.

Peucker, T.K., Douglas, D.H., 1975. Detection of surface specific points by local parallel processing of discrete terrain elevation data. Computer graphics and Image Processing 4, 375–387.

Ponce, V.M., Engineering Hydrology. Prince–Hall, New Jersey, 640p.

Reed, S.M., Maidment, D.R., 1995. A GIS procedure for merging NEXRAD precipitation data and digital elevation models to determine rainfall–runoff modeling parameters. Center for Research in Water Resources (CRWR), University of Texas at Austin Online Report 95–3, pp. 119.

Reed, S.M., Maidment, D.R., 1999. Coordinate transformations for using NEXRAD data in GIS–based hydrologic modeling, Journal of Hydrologic Engineering 4, 174–182.

Refsgaard, J., 1997. Parameterization, calibration and validation of distributed hydrological models. Journal of Hydrology 198 (1–4), 69–97.

Reitsma, R. F., Sautins, A. M., and Wehrend, S. C., 1994. Construction kit for visual programming of river–basin models. Journal of Computing in Civil Engineering 8(3), 378–384.

Remesan, R., Shamim, M., 2009. Runoff prediction using an integrated hybrid modeling scheme. Journal of Hydrology 372, 48–60.

Richardson, M.C., Branfireun, B.A., Robinson, V.B., Graniero, P.A., 2007. Towards simulating biogeochemical hot spots in the landscape: A geographic object–based approach. Journal of Hydrology 342(1–2), 97–109.

Ripley, D.B., 1981. Spatial Statistics. Wiley, New York, USA. 252pp.

Seo, D.J., Breidenbach, J.P., Johnson, E.R., 1999. Real–time estimation of mean field bias in radar rainfall data. Journal of Hydrology 223, 131–147.

Seo, D.J., Breidenbach, J.P., 2002. Real–time correction of spatially nonuniform bias in radar rainfall data using rain gauge measurements. Journal of Hydrometeorology 2, 93–111.

Shedd, R.C., Fulton, R.A., 1993. WRS–88D precipitation processing and its use in National Weather Service hydrologic forecasting. Proceeding of ASCE Internationa Symposiumon Engineering Hydrology.

Sherman, L.K., 1932. Streamflow from rainfall by unit graph method. Engineering News Record 108, 501–505.

Simanton, J.R. and Osborn, H.B., 1980. Reciprocal distance estimate of point rainfall. Journal of the Hydraulics Division, ASCE 106, 1242–1246.

Singh, V.P., Aravamuthan, V., 1996. Errors of kinematic–wave and diffusion–wave approximations for steady–state overland flows. Catena 27, 209–227.

Smith, C.J., 1986. The reduction of errors caused by bright bands in quantitative rainfall measurements made using radar. Journal of Atmospheric and Oceanic Technology 3, 129–141.

Smith, J.A., Krajeswski, 1991. Estimation of the mean field bias of radar rainfall estimates. Journal of applied Meteorology 30, 397–412.

Smith, J.A., Seo, D.J., Baeck, M.L., Hudlow, M.D., 1996. An intercomparison study of NEXRAD precipitation estimates. Water Resources Research 31, 2035–2045.

Smith, M.B., Seo, D. J., Koren, V.I., et al., 2004. The distributed model intercomparison project (DMIP); an overview. Journal of Hydrology 298(1–4), 4–26.

Stellman, K.M., Fuelberg, H.E., Garza, R., Mullusky, M., 2001. An estimation of radar and rain gauge–derived mean areal precipitation over Georgia watersheds. Weather Forecast 16, 133–144.

Tarboton, D.G., 1997. A new method for the determination of flow directions and upslope areas in grid digital elevation models. Water Resources Research 32, 309–319.

Thieken, A.H., Lucke, A., 1999. Scaling input data by GIS for hydrological modeling. Hydrologic Process 13(4), 611–630.

Troutman, B.M., Karlinger, M.R., Guerin, D.P., 1989. Basin–scale relations via conditioning. Stochastic Hydrology and Hydraulics 3, 111–133.

U.S Army Corps of Engineers (USACE), 1998. HEC–HMS hydrologic modeling system user's manual–version 1.0. Hydrologic Engineering Center, Davis, California.

Vazquez, R.F., Feyen, L., 2004. Potential evapotranspiration for the distributed modeling of Belgian basins. Journal of Irrigation and Drainage Engineering 130(1), 1–8.

Vertessey, R.A., Hatton, T.J., O'Shaughnessy, Jayasuriya, M.D.A., 1993. Predicting water yield from a mountain ash forest catchment using a terrain analysis based catchment model. Journal of Hydrology 150, 665–700.

Wang, J., Hassett, J.M., Endreny, T.A., 2005. An object oriented approach to the description and simulation of watershed scale hydrologic processes, Computers and Geosciences 31(4), 425–435.

Ware, E.C., 2005. Correction to radar–estimated precipitation using observed rain gauge data. MS thesis, Cornell University, Ithaca, 87.

Welch, G., Bishop, G., 2001. An Introduction to the Kalman Filter. SIGGRAPH 2001 course 8. In Computer Graphics, Annual Conference Graphics & Interactive Techniques. ACM Press.

Wilson, J.W., Brandes, E., 1979. Radar measurement of rainfall– A summary. American Meteorology Society 60, 1048–1058.

Wilson, J.P., gallant, J.C., 2000. Terrain Analysis: Principles and Applications. John Wiley and Sons: New York.

Winchell, M., Gupta, H.V., Sorooshian, S., 1998. On the simulation of infiltration and saturation excess runoff using radar–based rainfall estimates: Effects of algorithm uncertainty and pixel aggregation. Water Resources Research 34(10), 2655–2670.

Wise, S., 2000. Assessing the quality for hydrological applications of digital elevation models derived from contours. Hydrological Processes 14: 1909–1929.

Xie, H., Zhou, X., 2005. GIS–based NEXRAD Stage III precipitation database: automated approaches for data processing and visualization, Computers and Geosciences 31, 65–76.

Xie, H., Zhou, X., Hendricks, J., Vivoni, E., Guan, H., Tian, Y., Small, E., 2006. Evaluation of NEXRAD Stage III precipitation data over semiarid region. Journal of the American Water Resources Association 42(1), 237–256.

Young, C.B., Bradley, A.A., Krajewski, W.F., Kruger, A., Morrissey, M.L., 2000. Evaluating NEXRAD multisensor precipitation estimates for operational hydrologic forecasting. Journal of Applied Meteorology 14, 1430–1436.

Zhang, W., Montgomery, D.R., 1994. Digital elevation model grid size, landscape representation, and hydrologic simulations. Water Resources Research 30(4), 1019–1028.

Appendix A.

Local Bias Correction Procedure Used in Process 1 (P1)

In the simplest terms, the local bias correction procedure used in P1 may be described by the following:

$$r_c = r_0 \sum_{i=1}^{3} w_i \beta_i + \sum_{i=1}^{3} w_i \delta_i \qquad \text{Eq. A.1}$$

where

$$\beta_i = \begin{cases} 1 & \text{if } g_i / r_i > \beta_i \\ g_i / r_i & \text{if } g_i / r_i \le \beta_i \end{cases} \qquad \text{Eq. A.2}$$

$$\delta_i = \begin{cases} g_i - r_i & \text{if } g_i / r_i > \beta_i \\ 0 & \text{if } g_i / r_i \le \beta_i \end{cases} . \qquad \text{Eq. A.3}$$

In Eq. A.1, r_c denotes the bias–corrected radar rainfall (*mm*), r_0 denotes the raw radar rainfall at the bin centered at u_0 (*mm*), w_i denotes the weight given to the radar–gauge pair at the i^{th} vertex in the triangle of radar–gauge pairs that encloses u_0, β_i denotes the multiplicative sample bias from the ith radar–gauge pair, and β_i denotes the additive sample bias from the ith radar–gauge pair. In Eqs. A.2 and A.3, g_i and r_i denote the gauge rainfall measurement (*mm*) and the collocation radar rainfall estimate (*mm*), respectively, at the i^{th} vertex in the enclosing triangle, and β_i , an adaptable parameter, denotes the threshold for the multiplicative sample bias, g_i / r_i , i = 1,2,3. The neighboring

radar–gauge pairs are identified by “triangulation,” which connects all available radar–gauge pairs into a mesh of triangles. The weights, w_i, i = 1,2,3, sum to unity and are inversely proportional to the distance to the neighboring radar–gauge pairs in the enclosing triangle.

Appendix B.

Exponential Smoothing of Bin–Averaged Gauge Rainfall Using Gauge Measurements

The observation equation for the bin–average gauge rainfall centered at u_0 at hour k, G_{0k}, is given by

$$Z_{gk} = H_k G_{0k} + V_{gk} \qquad \text{Eq. B.1}$$

where the observation vector Z_{gk}; the structure vector H_k; the unknown bin–averaged gauge rainfall centered at u_0, G_{0k}; and the error vector V_{gk}; are given by $[g_{1k}, g_{2k}, g_{3k}, g_{4k}, g_{5k}, g_{6k}, \ldots\ldots, g_{(nk)k}]T$; $[1, 1, 1, 1, 1, 1, 1, 1, 1, 1, \ldots\ldots, 1]T$; $\|A_0\|^{-1} \int_{A0} P_k(u)du$; and $\left[G_{1k} - \|A_0\|^{-1} \int_{A0} P_k(u)du, G_{2k} - \|A_0\|^{-1} \int_{A0} P_k(u)du, ..., G_{nk} - \|A_0\|^{-1} \int_{A0} P_k(u)du\right]^T$, respectively. In the above, g_{ik} denotes the i^{th} rain gauge measurement at hour k, and $P(u)$ denotes the point hourly gauge rainfall at location u within the bin. The ij^{th} entry in the error covariance matrix of V_{gk}, Ψ_{gk} , is then given by

$$\Psi_{gijk} = \operatorname{cov}\left[G_{ik} - \|A_0\|^{-1} \int_{A0} P_k(u)du, G_{jk} - \|A_0\|^{-1} \int_{A0} P_k(u)du\right] \qquad \text{Eq. B.2a}$$

$$\begin{aligned}\Psi_{gijk} = {} & \|A_0\|^{-2} \int_{A0}\int_{A0} \operatorname{cov}\ P_k(u), P_k(v)\ dudv \\ & - \|A_0\|^{-1} \int_{A0} \operatorname{cov}\ G_{ik}, P_k(u)\ du \\ & - \|A_0\|^{-1} \int_{A0} \operatorname{cov}\left[P_k(u), G_{jk}\right]du + \operatorname{cov}\left[G_{ik}, G_{jk}\right]\end{aligned} \qquad \text{Eq. B.2b}$$

$$\Psi_{gijk} = \|A_0\|^{-1} \int_{A0} \gamma\ G_{ik}, P_k(u)\ du \qquad \text{Eq. B.2c}$$
$$+ \|A_0\|^{-1} \int_{A0} \gamma \left[P_k(u), G_{jk} \right] du$$
$$- \|A_0\|^{-2} \int_{A0} \int_{A0} \gamma\ P_k(u), P_k(v)\ du dv - \gamma \left[G_{ik}, G_{jk} \right],$$

where cov[] and γ[] denote the covariance and the semivariogram, respectively.

Appendix C.

Effect of Using Gauge Measurements, in lieu of Areally Averaged Gauge Rainfall, on Mean Square Error Calculations

The mean square error of raw radar–gauge estimates with respect to the gauge measurements, mse$[R_r - P(u)]$ is an estimate of $E\{[R_r - P(u)]^2\}$, where R_r denotes the raw radar rainfall and $P(u)$ denotes the gauge rainfall at some point u within the radar bin. We may rewrite $E\{[R_r - P(u)]^2\}$ as

$$E\{[R_r - P(u)]^2\} = E\{[R_r - G + G - P(u)]^2\}. \quad \text{Eq. C.1}$$

In the avove, G denotes the areally averaged gauge rainfall over the radar bin, that is, $G = \|A_0\|^{-1} \int_{A0} P(u)du$, where A_0 denotes the area of the bin. Then, under the assumption that the estimation error in the raw radar rainfall estimate, $R_r - G$, and the sampling error in the gauge measurement due to microscale variability of rainfall, $G - P(u)$, are linearly independent (Drake 1967; Ciach and Krajewski 1999 for justification), we may write

$$E\{[R_r - P(u)]^2\} \approx E[(R_r - G)^2] + \text{var}[G - P(u)]. \quad \text{Eq. C.2}$$

Likewise, under the similar assumption that $R_c - G$ and $G - P(u)$ are linearly independent, where R_c denotes the bias corrected radar rainfall, we may write

$$E\{[R_c - P(u)]^2\} \approx E[(R_c - G)^2] + \text{var}[G - P(u)]. \quad \text{Eq. C.3}$$

From Eqs. D.2 and D.3, we then have

$$E\{[R_r - P(u)]^2\} - E\{[R_c - P(u)]^2\} \approx E[(R_r - G)^2] - E[(R_c - G)^2] \qquad \text{Eq. C.4}$$

$$\frac{E\{[R_r - P(u)]^2\} - E\{[R_c - P(u)]^2\}}{E\{[R_r - P(u)]^2\}} < \frac{E[(R_r - G)^2] - E[(R_c - G)^2]}{E[(R_r - G)^2]} \qquad \text{Eq. C.5}$$

In other words, the true reduction in mean square error based on bin–averaged gauge rainfall, mse[$R_r - G$] – mse[$R_c - G$], is approximately the same as the apparent reduction, mse[$R_r - P(u)$] – mse[$R_c - P(u)$], based on rain gauge measurements, and the true percent reduction in mean square error based on bin–averaged gauge rainfall is larger than the apparent percent reduction based on rain gauge measurements.

VITA

Kwangmin Kang was born in Masan, South Korea. He received his Bachelor of Engineering degree from Kyonggi University, South Korea, and Master of Science degree from University of Florida, United States. He joined the Ph.D. program of Purdue University in August 2007.

LIST OF REFERENCES

APPENDICES

VITA